PHILOSOPHICAL TRANSACTIONS OF THE ROYAL SOCIETY B BIOLOGICAL SCIENCES

Molecular Dynamics Simulation of a Hydrated Phospholipid Bilayer

Jonathan W. Essex, Michael M. Hann and W. Graham Richards

Phil. Trans. R. Soc. Lond. B 1994 **344**, 239-260
doi: 10.1098/rstb.1994.0064

Molecular dynamics simulation of a hydrated phospholipid bilayer

JONATHAN W. ESSEX[1]*, MICHAEL M. HANN[2] AND W. GRAHAM RICHARDS[1]§

[1]*Oxford Centre for Molecular Sciences and Physical Chemistry Laboratory, University of Oxford, South Parks Road, Oxford OX1 3QZ, U.K.*
[2]*Glaxo Group Research, Greenford Road, Greenford, Middlesex UB6 0HE, U.K.*

SUMMARY

A hydrated bilayer of the phospholipid 1,2-dimyristoyl-sn-glycero-3-phosphorylcholine (DMPC) has been studied in the course of a molecular dynamics simulation. Comparison of the simulation results with experiment indicates that generally the two agree well. Data are presented concerning all the major system regions, including the hydrocarbon chains, the glycerol region, the lipid headgroups and the hydrating water molecules. The simulations suggest that this model can be extended to the study of more complex systems of greater biochemical interest, such as membrane bound proteins.

1. INTRODUCTION

Cell membranes are fundamental components of all biological systems (Stryer 1988), and as such obtaining a detailed understanding of their behaviour, on the atomic scale, is of considerable importance. Computer simulations can, in principle, provide such information, and this is reflected in the increasing number of such studies appearing in the literature. Simulations performed to date include those of membrane models (van der Ploeg & Berendsen 1982, 1983; Edholm & Nyberg 1992), micelles (Shelley *et al.* 1993; Wendoloski *et al.* 1989; Jönsson *et al.* 1986), hydrated monolayers (Alper *et al.* 1993; Charifson *et al.* 1990), bilayers (Egberts 1988; Egberts & Berendsen 1988; Berkowitz & Raghavan 1991; Damodaran *et al.* 1992; Damodaran & Merz 1993; Raghavan *et al.* 1992; De Loof *et al.* 1991), and oil/surfactant solutions (Karaborni *et al.* 1993). Phospholipids represent a particularly attractive simulation goal owing to their importance in biological membranes. In this paper, the behaviour of a hydrated bilayer of 1,2-dimyristoyl-sn-glycero-3-phosphorylcholine (DMPC), in the course of a molecular dynamics simulation, is analysed in detail and compared with experiment. In this manner it is hoped to justify the reliability of this simulation model as a predictive tool. The eventual goal of this work is the simulation of membrane bound proteins, and the study of pharmaceutically important processes such as the transport and partitioning behaviour of small molecules buried within the membrane.

The phospholipid selected for simulation, DMPC, is a zwitterionic molecule with two hydrocarbon chains, each containing 14 carbon atoms. Each hydrocarbon chain is physically distinct, and this should manifest itself in the simulation behaviour; the two hydrocarbon chains are referred to as S_n1 and S_n2. The molecule is shown as a schematic in figure 1. The water–lipid phase diagram for this system is complex (Janiak *et al.* 1979), showing a number of stable, distinct bilayer phases. The $P_{\beta'}$ and $L_{\beta'}$ phases are both gel phases in which the hydrocarbon chains are essentially frozen into an almost complete all-trans configuration, and the lipid molecules are close packed and tilted at an angle to the bilayer normal. Furthermore, in the $P_{\beta'}$ phase, the bilayers are rippled. At temperatures in excess of approximately 24°C, the L_α phase is adopted, corresponding to the liquid crystalline state in which the hydrocarbon chains are molten and the lipid molecules are free to diffuse in the plane of the bilayer. This phase is present in biological systems, and has therefore been selected as the simulation target. Furthermore, the L_α phase of this and related phospholipids has been extensively characterized by a wide range of experimental techniques, and it is essential to show that the simulation can reproduce these data.

2. METHODOLOGY

The intermolecular potential energy function outlined in equation (1) was selected for the simulations described here. Intramolecular degrees of freedom were described using Hooke's law terms for the bond-

* Present address: Department of Chemistry, Yale Univeristy, PO Box 208107, New Haven, Connecticut 06520-8107, U.S.A.
§ To whom correspondence should be sent.

Phil. Trans. R. Soc. Lond. B (1994) **344,** 239–260
Printed in Great Britain

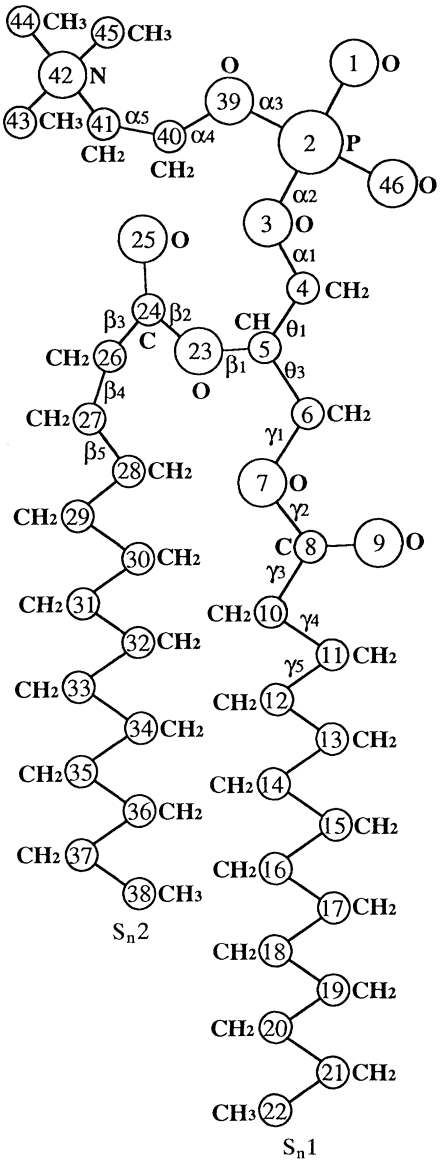

Figure 1. Schematic of the DMPC molecule. The group numbers given within the circles are used in table 1. The atoms constituting each group are shown in bold. The two hydrocarbon chains are labelled S_n1 and S_n2, and the dihedral angles used in the subsequent analysis are indicated. θ_3 corresponds to 4-5-6-7; θ_4 corresponds to 23-5-6-7.

stretching and angle-bending, and Fourier series for dihedral angle motion.

$$V = \sum_{\text{pairs}(i,j)} \frac{A_{ij}}{r_{ij}^{12}} - \frac{B_{ij}}{r_{ij}^{6}} + \frac{q_i q_j}{4\pi\epsilon r_{ij}}. \qquad (1)$$

A_{ij} and B_{ij} correspond to the Lennard-Jones coefficients for the van der Waals interactions between atoms i and j, r_{ij} is the distance between atoms i and j, and q_i is the charge on atom i.

The non-bonded parameters adopted for the lipid molecules were obtained from the Optimized Parameters for Liquid Systems (OPLS) united-atom parameter set provided with the BOSS 3.1 program (Jorgensen 1991). A series of disconnections were performed on the lipid molecule to generate fragments amenable to parameter transfer. For example, the electrostatic parameters for the $CH_2N(CH_3)_3$ moiety were obtained directly from the tetramethylammonium cation. It was noted during this work that the van der Waals parameters could be assigned to chemically distinct atom types within the OPLS force-field (Jorgensen & Tirado-Rives 1988), and as such are transferable. This procedure was therefore adopted in assigning the van der Waals parameters to the lipid system. In table 1, r^*, ϵ, atom centred electrostatic charge, q, and atom types for the lipid molecule are presented. The OPLS fragments from which the parameters are assigned are also marked, together with the atom names used in the subsequent analysis of the dynamics trajectories. At the boundaries between the fragments, the van der Waals parameters were modified, by analogy with the behaviour of the OPLS protein parameter set (Jorgensen & Tirado-Rives 1988), to take account of the change in connectivity. The combining rules adopted for the simulations were those implemented within the AMBER program (Singh *et al.* 1988), namely the arithmetic mean for the r^* values, and the geometric mean for the ϵ values. The OPLS force field uses the geometric mean for both components, although the difference is negligible in light of the crude parameterization scheme adopted here.

The use of this parameter assignment procedure relies on the assumption that the fragments can be treated as independent and non-interacting. This is unlikely to be true in the polar headgroup region of the lipid where a positively charged nitrogen group is approximately 5 Å from a negatively charged phosphate. However, use of this procedure is not without precedent (Charifson *et al.* 1990). Whereas the transferability of van der Waals parameters is regarded as a satisfactory procedure, as indicated above, the transfer of electrostatics is questionable. However, the alternative methods of electrostatic parameter generation have their own disadvantages. Ideally one would like to optimize the parameters to the results of full molecular dynamics simulations, although such an approach is too computationally demanding for this system. The use of *ab initio* calculations is a routine procedure (Chirlian & Francl 1987), although the presence of a phosphate anion in the lipid molecule necessitates the use of a basis set containing diffuse and polarization functions to reproduce its behaviour correctly (Hehre *et al.* 1986). *Ab initio* calculations at this level on the entire molecule are too demanding, whereas the use of a fragment approach in conjunction with *ab initio* calculations is not recommended for these systems (Stouch *et al.* 1991). Furthermore, the conformational dependency of the electrostatic parameters render their unambiguous assignment on the basis of the *ab initio* molecular electrostatic potential problematic (Stouch & Williams 1992; Reynolds *et al.* 1992). Thus although the parameter assignment procedure adopted in this work is crude, since charged fragments may polarize neighbouring groups, the alternative methods have their own difficulties; the approach adopted therefore constitutes an acceptable starting position.

PHILOSOPHICAL TRANSACTIONS OF THE ROYAL SOCIETY B BIOLOGICAL SCIENCES

Table 1. *Non-bonded parameters selected for the membrane simulation*

(The atom numbers correspond with those given in figure 1. Also presented are the OPLS fragments from which the parameters were derived, the names given to the various atoms in the subsequent analysis, and the atom types used in the assignment of intramolecular parameters. $Me_2PO_4^-$ is the dimethyl-phosphate anion, Me_4N^+ is the tetramethyl ammonium cation, MeOAc is methyl acetate, and hydrocarbon indicates that the parameters are derived from the hydrocarbon parameter set.)

atom number	r^*/Å	ϵ/kcal mol^{-1}	q	atom type	fragment	analysis name
1	1.661	0.210	−0.660	O2	$Me_2PO_4^-$	
2	2.099	0.200	0.780	P	$Me_2PO_4^-$	
3	1.684	0.170	−0.430	OS	$Me_2PO_4^-$	
4	2.133	0.118	0.200	C2O	$Me_2PO_4^-$	C
5	2.133	0.080	0.250	CH	MeOAc	
6	2.133	0.118	0.250	C2O	MeOAc	
7	1.684	0.170	−0.400	OS	MeOAc	
8	2.105	0.105	0.550	C	MeOAc	C1, S_n1
9	1.661	0.210	−0.450	O2	MeOAc	
10	2.192	0.118	0.050	C2	MeOAc	C2, S_n1
11 to 21	2.192	0.118	0.000	C2	hydrocarbon	C3 to C13, S_n1
22	2.192	0.175	0.000	C3	hydrocarbon	C14, S_n1
23	1.684	0.170	−0.400	OS	MeOAc	
24	2.105	0.105	0.550	C	MeOAc	C1, S_n2
25	1.661	0.210	−0.450	O2	MeOAc	
26	2.192	0.118	0.050	C2	MeOAc	C2, S_n2
27 to 37	2.192	0.118	0.000	C2	hydrocarbon	C3 to C13, S_n2
38	2.192	0.175	0.000	C3	hydrocarbon	C14, S_n1
39	1.684	0.170	−0.430	OS	$Me_2PO_4^-$	
40	2.133	0.118	0.200	C2O	$Me_2PO_4^-$	C_α
41	2.192	0.118	0.250	C2	Me_4N^+	C_β
42	1.824	0.170	0.000	N3	Me_4N^+	N
43 to 45	2.222	0.145	0.250	C3N	Me_4N^+	C_γ
46	1.661	0.210	−0.660	O2	$Me_2PO_4^-$	

It is necessary to consider whether a united-atom representation is capable of reproducing the complex behaviour observed in hydrated lipid bilayers. Whilst it has been shown that to reproduce the tilt-angle transitions in Langmuir-Blodgett films, an all-atom parameter set is required (Moller *et al.* 1991), in the simulations reported here the more open-packed L_α phase is simulated. Thus it does seem reasonable to select a united-atom parameter set as a starting point, thereby increasing simulation efficiency by removing all non-polar hydrogen atoms from the simulation.

The bond-stretching, angle-bending, and dihedral energy terms are taken directly from the AMBER force-field (Weiner *et al.* 1984), where the parameters are available. This procedure is recommended when applying the OPLS force field to protein simulations (Jorgensen & Tirado-Rives 1988). Non-bonded 1,4 interactions are included in the evaluation of the dihedral energy term, the van der Waals contribution being reduced by a factor of eight and the electrostatics by a factor of two, as recommended for the OPLS parameter set when used in conjunction with AMBER (Jorgensen & Tirado-Rives 1988). Two 'improper' torsions are defined in thelipid molecule. The first enforces a tetrahedral geometry at the chiral centre; because a united-atom representation is being employed, it is not inconceivable that a chiral centre will racemize in the course of a molecular dynamics simulation, unless a restraining function is employed. The second 'improper' torsion enforces planarity of the ester groups.

The AMBER force-field does not contain the necessary functions to treat the ester groups within the lipid. The required parameters were obtained from two sources. The bond-stretching and angle-bending parameters were taken from the paper by Charifson *et al.* (1990) in which the molecular mechanics parameters were obtained by comparison with *ab initio* calculations on methyl acetate at the 6-31G* level. The dihedral energy parameters were derived from the OPLS methyl acetate parameters (Jorgensen *et al.* 1990). This was achieved using a series of constrained minimizations to determine firstly the contribution to the dihedral energy barrier arising from 1,4 non-bonded interactions, and secondly, the appropriate Fourier series coefficients to reproduce the OPLS barrier with the inclusion of the 1,4 interactions. All non-standard AMBER intramolecular parameters, together with the associated potential energy functional forms, are given in Appendix 1.

A hydrated lipid bilayer consisting of 36 zwitterionic 1,2-dimyristoyl-sn-glycero-3-phosphorylcholine (DMPC) molecules and 1560 TIP3P water molecules (Jorgensen *et al.* 1983) was generated within AMBER version 3.1 (Singh *et al.* 1988). This system composition contains approximately 50% water by mass, and therefore at temperatures in excess of 24°C lies within the L_α-excess water region of the phase diagram

PHILOSOPHICAL TRANSACTIONS OF THE ROYAL SOCIETY B BIOLOGICAL SCIENCES

(Janiak *et al.* 1979). Hence the simulated system should behave as an isolated unilamellar bilayer.

The starting geometry selected for the simulations was a modification of the crystal structure (Pearson & Pascher 1979). The structure has the monoclinic space group $P2_1$, with cell parameters: 8.72 Å, 8.92 Å, 55.4 Å, $\beta = 97.4°$. The asymmetric unit contains two conformationally distinct lipid molecules (referred to as A and B), displaced by 2.5 Å in the direction of the bilayer normal. The hydrocarbon chains are inclined at an angle of 12° to the bilayer normal, and the system has a headgroup surface area of 38.9 Å^2. A program was written to convert the fractional crystallographic coordinates of the asymmetric unit, as provided by the authors, into systems of any specifed size within cartesian space.

It is unreasonable to expect a hydrated bilayer packed as per the crystal geometry to enter the L_α region of the phase diagram in the course of a molecular dynamics simulation. For this reason the X-ray structure was modified to render the passage to the L_α phase as trivial as possible. The modifications performed on the crystal structure are as follows:

1. The angle of tilt of each molecule was modified by 15° to render the hydrocarbon chains approximately parallel to the bilayer normal. The X-ray structure resembles the rippled P_β, phase in that the hydrocarbon chains are both ordered and tilted, and that the lipids are displaced with respect to each other in a zig-zag fashion. The rotation of the lipid molecules is therefore an attempt to avoid entering this phase.

2. The two molecules of the asymmetric unit were translated such that the displacement of the phosphorus atoms along the bilayer normal was reduced to 0.5 Å. Again, this was done to ensure that the system did not enter the P_β, phase.

3. The phosphorus–phosphorus separation across the bilayer was reduced to approximately 35.6 Å, in broad agreement with the experimental value of 34.0 ± 1.0 Å for the L_α phase (Lewis & Engelman 1983).

4. The separation between each lipid molecule was increased to generate a headgroup surface area of 63.8 Å^2. There are five experimental values available for this property evaluated either using X-ray diffraction or deuterium nuclear magnetic resonance (NMR). Lewis & Engelman (1983) obtained the value 65.7 ± 3.0 Å^2 using X-ray diffraction on unilamellar vesicles at 36°C. Janiak *et al.* (1979) evaluated the headgroup surface area of DMPC at a range of temperatures from the P_β,/L_α phase transition of 24°C, up to 45°C, using X-ray diffraction. The headgroup surface area was observed to increase from 58 Å^2 to 63 Å^2. Lis *et al.* (1982) obtained a value of 65.2 Å^2 at 27°C using X-ray diffraction, and the diffraction data of Hui & He (1983) can be interpreted to give surface areas of 61 Å^2 or 66 Å^2, depending on the choice of hydration data (De Young & Dill 1988). Deuterium NMR have been interpreted to give headgroup surface areas of 67 Å^2 and 72 Å^2, at 25°C and 45°C, respectively (De Young & Dill 1988). Clearly, there is considerable experimental uncertainty in the headgroup surface area. The value adopted in the simulations is within the range of experimental values derived from X-ray diffraction. The system size was not increased uniformly along the two dimensions (x and y) of the lipid plane. This is because in the asymmetric unit two lipid molecules lie adjacent to the x axis, whereas only one molecule lies adjacent to the y axis. Hence, the system dimensions were expanded such that the lipidlipid separations along the two dimensions are broadly equivalent, and thus the x dimension of the simulation box is greater than that of the y. The system dimensions were set at 35.598 Å, 32.242 Å, 77.661 Å, corresponding to a $3 \times 3 \times 1$ replication of the unit cell.

The lipid bilayer generated using the above protocol was hydrated within a modified version of the EDIT module. TIP3P water (Jorgensen *et al.* 1983) was placed into the system using a simple collision test. Thus if any lipid atom was within 2 Å of a water oxygen, then that water molecule was discarded. Water was allowed to penetrate into the bilayer to a sufficient depth to ensure hydration of the glycerol carbonyl groups. The presence of water at this depth within the membrane has been confirmed by at least three experimental sources (Fringeli & Günthard 1976; Blume *et al.* 1988; Blechner *et al.* 1990). It is conceivable that the collision diameter selected for the hydration process was too small, and that the extent of initial water penetration was too great. However, the phosphorusphosphorus separation was observed to relax close to the experimental value in the course of molecular dynamics, and thus the hydration scheme is probably satisfactory.

A dummy atom of mass 10 atomic mass units was added to the lipid region of the simulation to act as a solute. This atom has non-bonded parameter values of $r^* = 0.4$ Å, $\epsilon = 0.0$ kcal mol^{-1}, $q = 0.0$, and therefore does not interact with the rest of the system. In the course of the simulations, the dummy's velocity was set to zero. This non-interacting dummy atom was added since AMBER is designed for the simulation of dilute solutions, and thus a solute molecule is required. The use of a dummy atom fulfills this requirement, without significantly modifying the system behaviour.

The simulation system was energy minimized within AMBER prior to performing molecular dynamics. The minimization was done in a stepwise fashion. Initially, only the hydrogen atoms were minimized, then the water molecules, and finally the system as a whole.

In this, and all subsequent simulations, a residue based cutoff of 8 Å was adopted, where each residue is an entire lipid molecule. Thus if any two lipid atoms were within 8 Å, then the entire lipid–lipid interactions were evaluated. The use of such a short cutoff is clearly a significant weakness of these simulations. Furthermore, the non-bonded cutoff is implemented in AMBER such that although the pair list is evaluated on a residueresidue basis, periodic boundary conditions are applied separately to the individual atom–atom interactions. The possibility of this procedure introducing simulation artefacts by splitting lipid

PHILOSOPHICAL TRANSACTIONS OF THE ROYAL SOCIETY B BIOLOGICAL SCIENCES

dipole moments needs to be remembered. Ideally, it would be preferable to adopt a larger simulation system, although limitations on the available computer time render this extension impossible. It should be borne in mind that for most liquid phase simulations of small molecules, a short non-bonded cutoff of the order of 8 Å is routinely used (Jorgensen 1989). In the case of charged systems, however, this cutoff is generally regarded as too short since the electrostatic interactions decrease as r^{-1}, where r is the interparticle separation. The molecules in these simulations are electrically neutral, but are also zwitterionic and therefore highly polar; dipoledipole interactions decrease as r^{-3}. Hence the electrostatic truncation problem, although very real, is not as severe as a first impression might indicate. Clearly, however, any extension of the simulations reported here should treat the inclusion of long-range electrostatics as a high priority, using either a reaction field (Egberts & Berendsen 1988) or an Ewald lattice sum (Allen & Tildesley 1987). The truncation of electrostatic interactions at 8 Å is likely to have a significant effect on correlated molecular behaviour, such as the dielectric constant (Allen & Tildesley 1987), and this should be remembered when considering the simulation results. However, static structural and thermodynamic averages of simple fluids are generally not sensitive to the inclusion of long-range electrostatic interactions (Alper & Levy 1989), although recent simulations of water above a phospholipid monolayer by Alper *et al.* (1993) suggest that cutoffs in excess of 30 Å are required for simulation artefacts to be avoided. Cutoffs of this magnitude were impossible to implement owing to limited computational resources.

The minimized system was equilibrated using the GIBBS module of AMBER for 10 ps at 323.15 K, under constant number–volume–temperature (NVT) conditions, the lipid atoms being constrained to their minimized positions. A timestep of 0.005 ps was adopted during this phase, the simulation aim being to relax the water molecules in the vicinity of the polar headgroups. The simulation temperature was constrained using the Berendsen algorithm (Berendsen *et al.* 1984) in conjunction with a relaxation time of 0.005 ps. In this and all subsequent simulations, the bond lengths were constrained to their equilibrium values using the SHAKE algorithm (Ryckaert *et al.* 1977) thereby allowing the use of a larger timestep, without significantly biasing the molecular dynamics trajectory (van Gunsteren & Karplus 1982). Also, the non-bonded pair list was updated every 10 steps.

In the course of this and the equilibration simulations, the atomic mass of the water hydrogen atoms was increased to 16 atomic mass units, as per the protocol of Egberts (1988). The effect of this mass increase is to eliminate the librational motion of the water molecules, thereby allowing the use of a larger timestep in conjunction with the SHAKE constraint algorithm. Thermodynamic averages are unaffected by modification of mass as these properties are a function of the potential energy of the system, although their rates of convergence will, of course, be reduced (Pomès & McCammon 1990). Thus during the equilibration phase of the simulation, 'heavy' water was adopted.

Subsequent to the 10 ps water relaxation simulation, 200 ps of molecular dynamics on just the lipid molecules was performed under constant NVT conditions, at a temperature of 323.15 K, with a timestep of 0.004 ps. This simulation was done in an attempt to ensure that the hydrocarbon chains were 'melted', as required for a membrane system in the L_α region of the phase diagram. Molecular dynamics was then performed on the whole system, again under constant NVT conditions at a temperature of 323.15 K with a timestep of 0.004 ps. Four hundred picoseconds of equilibration preceded 150 ps of a production simulation, the latter being performed with normal hydrogen masses and a time step of 0.002 ps. These simulations were performed using a modified version of the GIBBS module, altered in such a way that the lipid and water phases were coupled to independent temperature baths. In this manner it was hoped to eliminate the possibility of local heating effects occurring, as has been observed elsewhere (Damodaran & Merz 1993). System coordinates were stored every 1 ps for post-processing, except in the final 20 ps of the production simulation, when they were stored every 0.2 ps.

3. RESULTS AND DISCUSSION

The static and dynamic behaviour of the system will be compared with the available experimental data. Only a selection of the data from the 400 ps equilibration phase will be presented to illustrate convergence; the final 150 ps production simulation will be analysed more fully. Furthermore, attempts will be made to justify the simulation behaviour in all regions of the anisotropic simulation system.

(*a*) *Hydrocarbon region*

The average orientational order of each methylene chain segment within the hydrocarbon region can be defined in terms of an order parameter, S, where S is defined in equation (2).

$$S = 0.5 < 3\cos\vartheta_i \cos\vartheta_j - \delta_{ij} > . \qquad (2)$$

ϑ_i represents the angle between then ith molecular axis and the bilayer normal, and δ_{ij} is the Kronecker delta function. The term in $< \ldots >$ corresponds to the appropriate ensemble average. In this case, the bilayer normal corresponds to the system z axis. Deuterium NMR enables the direct evaluation of the experimental order parameter, S_{CD}, reflecting the average orientation of the C—D bond vector with respect to the bilayer normal. The order parameters can take values ranging from 1 to −0.5, depending on the molecular orientation; a value of 0 probably indicates full isotropic motion of the group in question. The united-atom simulations described here can be analysed to give the order parameter S_{CD} using the following procedure (Egberts & Berendsen 1988). For nth methylene segment, three

orthogonal vectors are defined: (i) z, vector from C_{n-1} to C_{n+1}; (ii) y, vector perpendicular to z and in the plane of C_{n-1}, C_n and C_{n-1}; and (iii) x, vector perpendicular to z and y. The experimental order parameter, S_{CD}, is related to the order parameters derived using the above vector definitions as follows.

$$S_{SD} = 2S_{xx}/3 + S_{yy}/3. \quad (3)$$

The order parameter S_{zz} corresponds to the orientation of each individual methylene segment.

The values of S_{CD} observed in the course of the final 100 ps of molecular dynamics on just the lipid molecules, together with the production simulation results, are presented in figure 2, for the S_n1 chain, and figure 3 for the S_n2 chain, respectively. The experimental data selected (Seelig & Seelig 1974; Oldfield *et al.* 1978) are the most relevant for the system in question; the order parameters are not explicitly given, but the quadrupolar splittings have been used in the manner described by Seelig & Seelig (1974). Where the experimental deuteration of the hydrocarbon chains was not selective, the assumption was made that the S_n2 chain is more disordered than the S_n1, although the experimental evidence for this is contradictory (Cevc & Marsh 1987; Davis 1979, 1983; Thurmond *et al.* 1991). It can be seen from the figures that there is a plateau in the experimental order parameter profile in the region of C3 to C10. This profile has been interpreted in terms of an intermolecular restriction on the allowed chain conformations (Cevc & Marsh 1987). It is also of note that the nature of the phosphatidylcholine appears to have little effect on the overall shape of the profile, provided the hydrocarbon chains are fully saturated, and therefore the more complete data sets derived from dipalmitoyl phosphatidylcholine (DPPC, C16 hydrocarbon chains) can be used for comparison with the simulation results. The C2 methylene group order parameters are chain dependent. This has been interpreted in terms of the bend at the top of the S_n2 chain in the crystal structure being conserved in the hydrated system, resulting in the orientational behaviour of the C2 methylene hydrogen atoms being considerably different to those of the rest of the hydrocarbon chain (Cevc & Marsh 1987). Furthermore, the C2 methylene group of the S_n2 chain has two discrete values. There are two possible interpretations for this behaviour. Firstly, the methylene group resides in two distinct long lived conformations, or secondly, the methylene group resides in only one conformation, but the two protons undergo different motional averaging. Selective deuteration at this site indicates that the latter is the correct interpretation (Engel & Cowburn 1981).

It is apparent from inspecting figures 2 and 3 that the agreement with experiment is poor for the simulations in a constrained water environment; there is considerably more order in the hydrocarbon region than experiment indicates. However, there are a number of points of note. The anomalous behaviour of the C2 methylene segment of the S_n2 hydrocarbon chain is reproduced; this group has a value lower than the order parameter plateau. This is consistent with the explanation offered above; in these simulations, the rigid water matrix locks the methylene group into the crystallographic conformation.

The agreement between the experimental order parameters and the results obtained from the production simulation is excellent. Furthermore, a consideration of the difference in simulation and experimental conditions improves the agreement. For the S_n1 chains, the final order parameters are slightly smaller than experiment; this is consistent with the experimental data having been obtained on DPPC at a temperature 16°C in excess of the main phase transition temperature (Seelig & Seelig 1974). The simulations are performed on the DMPC system with a temperature approximately 26°C above the main phase transition, and the corresponding order parameters are therefore expected to reflect greater disorder than the experimental data. The converse is true of the S_n2 experimental data (Oldfield *et al.*

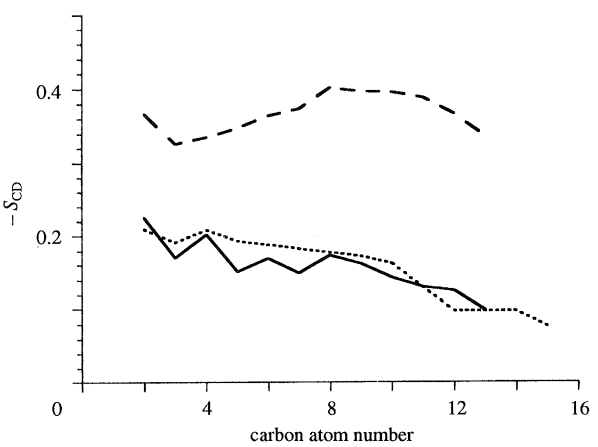

Figure 2. Simulation and experimental S_n1 order parameters. Experimental data (Seelig & Seelig 1974) correspond to that of dipalmitoyl phosphatidylcholine (DPPC) at 57°C. Dashed line, 100–200 ps, lipid only; solid line, production simulation; dotted line, experiment.

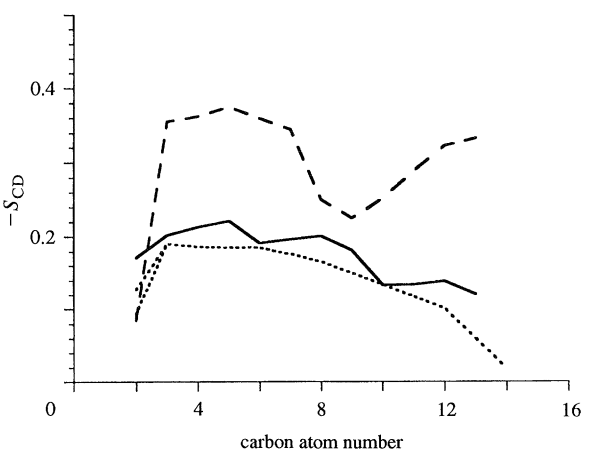

Figure 3. Simulation and experimental S_n2 order parameters. Experimental data (Oldfield *et al.* 1978) correspond to that of dimyristoyl phosphatidylcholine (DMPC) at 60°C. Dashed line, 100–200 ps, lipid only; solid line, production simulation; dotted line, experiment.

PHILOSOPHICAL TRANSACTIONS OF THE ROYAL SOCIETY B BIOLOGICAL SCIENCES

1978), since the experimental order parameters are obtained from DMPC at 60°C, and should therefore be smaller than the simulation results. For the S_n1 order parameters, the root mean squared (r.m.s.) deviation between simulation and experiment is 0.02, whereas for the S_n2 chain, the r.m.s. deviation is 0.04. However, for the latter, the agreement is particularly poor at the C2 methylene group; excluding this group from the analysis reduced the r.m.s. deviation to 0.03. It should be noted that in evaluating the r.m.s. deviations, only those methylene segments with experimental data are used; the experimental data are incomplete, but no attempt to use interpolated values has been made. Analysis of the order parameters for the equilibration simulation suggests that this simulation property appears converged in the last 200 ps of this simulation. The r.m.s. deviations between the order parameters of the 200–300 ps and 300–400 ps equilibration simulations are 0.02 and 0.03 for the S_n1 and S_n2 hydrocarbon chains, respectively. Thus the statistical uncertainty in the values derived from the production simulation is of this order, and the production simulation results therefore agree with experiment to within the simulation error bounds. Error estimation using the standard error on batch averages of the production simulation order parameters is potentially problematic; the data may be correlated, thereby yielding an artificially low error estimate. Thus the approach adopted above, while crude, is arguably adequate. It is apparent from both sets of figures that the simulation S_n2 parameters are, on average, larger than the corresponding S_n1 parameters; the r.m.s. deviation between the two data sets is 0.03, although the statistical uncertainty in the data is such that this difference may not be systematic.

The production simulation does not reproduce the C2 order parameter of the S_n2 hydrocarbon chain, unlike the simulations with constrained water. However, the remainder of the profile reproduces the experimental data very well. It should be noted that the processing of the simulation data implicitly assumes that the motional averaging about each CD bond is equivalent, and experiment suggests that this is not true of the C2 segment of the S_n2 chain (Engel & Cowburn 1981). Furthermore, if the two C2 order parameters arise from the presence of two conformations in the S_n2 chain at this point, then potentially the simulations may be sampling only one conformation; this explanation was offered by Egberts (1988) to explain the same observation. Brownian dynamics simulations (De Loof *et al.* 1991) show the anomalous behaviour of the C2 segment of the S_n2 chain, although the data at this point are not considered converged, even after nanoseconds of simulation. Furthermore, the Brownian dynamics simulations make approximations regarding the behaviour of the headgroups, and completely neglect electrostatic interactions. Clearly, reproducing experiment at this particular chain segment is problematic.

In the simulations by van der Ploeg & Berendsen (1982) of a decanoate bilayer, a collective hydrocarbon chain tilt was observed to occur over the length of the periodic simulation system. It is therefore appropriate to investigate the equivalent behaviour in the simulations reported here. An average tilt vector, $\boldsymbol{T}$, is defined as in equation (4).

$$T = 1/N \sum \boldsymbol{S}_i. \tag{4}$$

The summation is performed over the N hydrocarbon chains in the simulation system. $\boldsymbol{S}_i$ corresponds to the chain vector of the ith hydrocarbon chain, defined such that $\boldsymbol{S}_i$ links atom 1 of hydrocarbon chain i to atom 14 of the same chain. The $\boldsymbol{S}_i$ vectors are normalized. A large value of $\boldsymbol{T}$ indicates that there is a strong correlation between the tilt vectors, $\boldsymbol{S}_i$. Moreover, from the tilt vector $\boldsymbol{T}$ it is possible to evaluate the average tilt angle for the entire lipid system.

In figure 4 the behaviour of the modulus of the collective tilt vector $\boldsymbol{T}$, together with the average angle with respect to the z axis derived from the individual vectors $\boldsymbol{T}_i$, and the angle with respect to the z axis of the collective tilt vector, are presented as a function of simulation time for layer 1 of the lipid bilayer during the production simulation. Inspection of the equivalent data for layer 2 indicates that the tilt behaviour of the $\boldsymbol{S}_i$ vectors is largely identical in the two halves of the bilayer. However, the collective tilt, $|\boldsymbol{T}|$, is consistently larger in layer 1 than layer 2, as is the tilt angle derived from $\boldsymbol{T}$, and moreover changes little in the course of the 150 ps production simulation. The final value of the collective tilt angle is 4° in layer 2. It therefore seems likely that a substantial cooperative tilt is occurring in layer 1, but not in layer 2. A possible explanation of this effect is the presence of a pronounced ripple in this half of the lipid bilayer, in which several of the lipid molecules are pushed towards the centre of the hydrocarbon region. This analysis suggests that at least one half of the lipid bilayer is showing a cooperative tilt, and that therefore the simulations system is arguably too small. Ideally, a simulation system with dimensions in excess of twice the correlation length of the cooperative tilt should be used, although this would be prohibitively expensive; the appropriate simulation

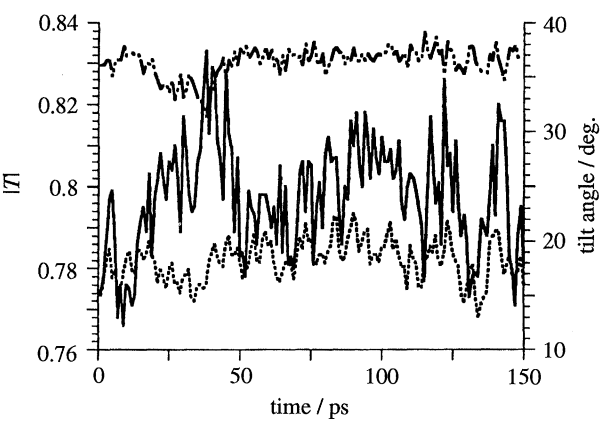

Figure 4. Behaviour of the modulus of the collective tilt vector $|\boldsymbol{T}|$, together with the tilt angles derived from $\boldsymbol{T}$ and the individual chain vectors $\boldsymbol{S}_i$, for layer 1 of the lipid bilayer. Solid line, $|\boldsymbol{T}|$; dot-dashed line, $\boldsymbol{S}$ tilt; dotted line, $\boldsymbol{T}$ tilt.

PHILOSOPHICAL TRANSACTIONS OF THE ROYAL SOCIETY B BIOLOGICAL SCIENCES

system needed for testing would be approximately 60 Å by 60 Å in the bilayer plane. It should, however, be stressed that the methylene order parameters are sensitive to the extent of chain tilting, and that therefore the agreement of this property with experiment should be sufficient to justify the tilt behaviour of the hydrocarbon region. Whilst van de Ploeg & Berendsen (1983) noted the loss of cooperative tilt on increasing the simulation system size, other system properties appeared insensitive to the presence of cooperativity. This is consistent with the observed agreement between simulation and experimental order parameters. The difference in tilt behaviour observed in the two halves of the bilayer system does not necessarily indicate that the system is out of equilibrium, but merely that simulations in excess of 550 ps are needed to ensure that equilibrium has been reached; the cooperative tilt may be an acceptable thermal fluctuation.

The dynamic behaviour of the hydrocarbon chains can be analysed using the autocorrelation function (van der Ploeg & Berendsen 1983), $C(\tau)$, of the tilt vectors $\boldsymbol{S}_i$:

$$C(\tau) = < \boldsymbol{S}_i(t)\boldsymbol{S}_i(t+\tau) > . \qquad (5)$$

$\boldsymbol{S}_i(t)$ corresponds to the individual chain vector i at time t, and $\boldsymbol{S}_i(t+\tau)$ corresponds to the same chain vector at time $(t+\tau)$. Fitting a single exponential function to the entire autocorrelation function gives correlation times of 1185 ps for the vectors $\boldsymbol{S}_j$, and 374 ps and 450 ps for the x and y components, respectively. The length of these correlation times means that ideally simulations in excess of 500 ps are needed to reproduce the full dynamic behaviour of the hydrocarbon region. Whether these numbers are physically realistic should be addressed; simulation of a decane bilayer (van der Ploeg & Berendsen 1983) give a considerably shorter correlation time of 8 ps. However, Brownian dynamics simulations (De Loof *et al.* 1991) give a correlation time of the order of 500 ps for the wobbling motion of individual phospholipid hydrocarbon chains, in qualitative agreement with the values reported here. Furthermore, NMR data can be interpreted in terms of correlation times of the order of nanoseconds for collective lipid reorientations (Meier *et al.* 1986; Rommel *et al.* 1988). It must, of course, be noted that the correlation times given above are considerably longer than the length of the simulation from which they were derived, and consequently have a large statistical uncertainty. The simulation correlation times must therefore be regarded as giving an order of magnitude estimate only. However, the behaviour of the hydrocarbon chain vectors suggests that the use of a larger simulation system, in conjunction with significantly longer simulations, is required to sample fully the phase space accessible to the hydrocarbon region.

It is apparent that if the bilayer is to achieve the experimentally observed dimensions, then gauche conformations within the hydrocarbon chains are a necessity. Furthermore, if the standard model of the L_α hydrocarbon region as essentially molten is correct, one would expect gauche conformations to be present. There are a number of experimental methods for determining the transgauche populations within the bilayer, namely Raman spectroscopy (Pink *et al.* 1980), NMR (Meier *et al.* 1983) and infra-red spectroscopy (Mendelsohn *et al.* 1989). The correlation times for the isomerization process can also be estimated from the observed NMR relaxation times (Meier *et al.* 1986). Clearly, a successful membrane model should be able to reproduce not only the equilibrium conformational populations, but also the correlation times describing the rate at which the isomerizations occur.

Mendelsohn *et al.* (1989) analysed the CD_2 rocking frequency of selectively deuterated DPPC at a temperature of 48.5°C, and obtained values for the gauche conformation populations at C4, C6 and C10. These data were interpreted to indicate the presence of approximately 7.2 gauche conformations per lipid molecule of DPPC in the L_α phase. Subsequent work (Mendelsohn *et al.* 1991) performed at 50°C gave gauche populations at C4, C6, C10, C13, and C14/15. Pink *et al.* (1980) analysed the spectral intensity of the 1130 cm^{-1} skeletal vibration using Raman spectroscopy, and determined, with the aid of a model, that DPPC has approximately 10.5 gauche conformations per molecule at 50°C. The model was then adapted to predict the conformational behaviour of DMPC as a function of temperature, and gave between 7.5 and 8.0 gauche conformations per molecule at 50°C. The approximations adopted in this analysis have subsequently been criticized (Mendelsohn *et al.* 1989), and therefore the infra-red spectroscopy data are perhaps the more reliable. Density measurements (Nagle & Wilkinson 1978) have been used to determine a value for the number of gauche conformations per DPPC molecule for the L_α phase, namely, 7.6. Analysis of the order parameter results (Seelig & Seelig 1974) obtained from selectively deuterated DPPC give a value of between 6 and 12 gauche isomers per molecule.

Nuclear magnetic resonance relaxation measurements, using both deuterated and normal lipids, can be analysed to give conformational distributions, and also the correlation times for transgauche isomerization. Meier *et al.* (1986) determined the correlation times for transgauche isomerization of selectively deuterated DMPC at 323 K; values of the order of 100 ps were obtained. Also, a mobility gradient within the hydrocarbon chains corresponding to decreasing isomerization rates on approaching the end of the hydrocarbon chains was observed. The work of Brown *et al.* (1979) confirmed this; the correlation times in the region C3–C9 of DPPC at 51°C are constant, with a value of approximately 100 ps, and then decrease towards the chain terminus with a value of approximately 10 ps. Furthermore, the data suggest that the C2 methylene segments show larger correlation times than their neighbours (approximately 120 ps), and this should be reproduced in the simulations. Mayer *et al.* (1988) used specifically deuterated DMPC to determine the transgauche correlation times of the hydrocarbon chains. The values determined are 500 ps at C2, 10 ps at C6, and 1 ps at C13. These

PHILOSOPHICAL TRANSACTIONS OF THE ROYAL SOCIETY B BIOLOGICAL SCIENCES

values were obtained by interpolation from a figure in this paper, and correspond to a temperature of 323 K. Furthermore, relaxation studies of the C2 segment of the S_n2 chain give the following conformation populations for this segment at 308 K: 8% trans, 68% gauche$^+$ and 24% gauche$^-$. Rommel *et al.* (1988) used proton NMR on DMPC at 303 K to estimate a transgauche isomerization time of 200 ps. The study of fluorinated DMPC suggests a correlation time of the order of 100 ps for transgauche isomerization (Peng *et al.* 1988). Fuson & Prestegard (1983) report a transgauche correlation time for the C2–C3 torsion of the S_n2 hydrocarbon chain of 620 ps. The work of Meier *et al.* (1986) confirms the predicted increase in gauche conformations on approaching the bilayer centre. Meier *et al.* (1983) give a gauche population of 35% for the final torsion of DMPC at the main phase transition temperature.

The spread of the experimental correlation times suggests that the accuracy with which these values are known is poor. However, the data suggest that the correlation times should be of the order of 100 ps, and decrease on approaching the chain terminus. It is of interest to note that Brownian dynamics simulations on heptane (Levy *et al.* 1979) give dihedral correlation times consistent with those reported above, namely 101 ps for an outer dihedral, and 141 ps for the inner dihedral.

In the following analysis of the simulation trajectories, a conformation is assigned trans if it has a dihedral angle of $180 \pm 60°$, gauche$^+$ with an angle of $60 \pm 60°$, and gauche$^-$ with an angle of $-60 \pm 60°$. The average gauche population of the production simulation corresponds to $27.8 \pm 2.3\%$. The data of Mendelsohn *et al.* (1989, 1991) correspond to an average gauche population for DPPC of $24.2 \pm 2.8\%$ at 48.5°C, and 25.6% at 50°C. If the dihedral angles about C1–C2 and C2–C3 are excluded from the simulation analysis, then a value of $23.5 \pm 1.9\%$ is obtained. The exclusion of the first two dihedrals from the simulation analysis is justified as the experimental analysis did not include any atom involving these dihedrals, and furthermore these torsions have a tendency for showing an increased gauche population for reasons of bilayer packing. The errors reported for the simulation populations are derived from the standard deviations of the mean gauche$^+$–gauche$^-$ populations.

In table 2, the gauche populations for the carbon atoms C4, C6, C10, C11, and C12/13 are presented, together with the experimental data of Mendelsohn *et al.* (1989, 1991). The experimental populations of C13 and C14/15 are compared with the simulations values for C11 and C12/13, since the simulated lipid contains two less carbon atoms per chain. The simulation values were obtained from the average of the gauche populations of the two torsions involving the relevant carbon atom. The simulation errors are the standard deviation of the individual gauche populations contributing to this average. Simulation and experiment only agree to within the error bounds at C4 and C10. The gauche population of C12–C13 also differs markedly from the prediction of Meier *et al.* (1983) of 35%. The failure of the simulation to reproduce the experimental mobility gradient predicted from NMR studies is not unexpected; the simulation statistics are rather poor, and furthermore this subtle behaviour is likely to be very dependent on parameter selection and simulation conditions. Moreover, the difference in simulation and experimental conditions is a further complication. However, it is interesting to note that the infra-red data (Mendelsohn *et al.* 1989, 1991) do not show any such gradient.

Table 2. *Simulation and experimental (Mendelsohn* et al. *1989, 1991) gauche populations as a function of methylene segment position*

carbon atom number	experiment/ 48.5°C	experiment/ 50°C	simulation
C4	20.7 ± 4.2	21.0	22.2 ± 7.4
C6	32.3 ± 2.3	30.0	26.0 ± 3.5
C10	19.7 ± 0.8	20.0	24.1 ± 4.7
C13 (C11)		17.0	23.9 ± 3.9
C14/C15 (C12/13)		40.0	23.3 ± 4.0

In figures 5 and 6, the transgauche populations are presented as a function of torsion number for the S_n1 and S_n2 hydrocarbon chains of the production simulation. The torsions are defined such that C1–C2 is torsion 1, C2–C3 is torsion 2, etc. Oscillations in the trans populations are observed; it is interesting to note that Brownian dynamics simulations (De Loof *et al.* 1991) also show an oscillation in trans population as a function of carbon atom number. Because these simulations extend over the nanosecond timescale, the observed oscillations reported here are arguably not due to the comparatively short simulation time. The odd-even alternation in population was also observed by Egberts & Berendsen (1988), and ascribed to the preferred alignment of the hydrocarbon chain parallel to the bilayer normal. The prediction of increasing gauche conformation probability with increasing torsion number is not reproduced, although the simulation errors, as determined by the difference in gauche$^+$–gauche$^-$ probabilities, render the data too

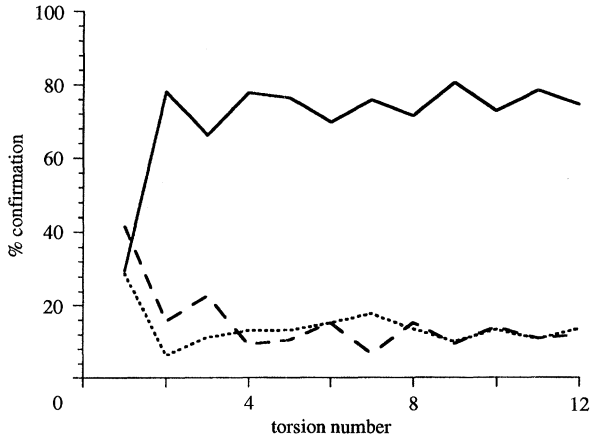

Figure 5. Conformational populations for the S_n1 hydrocarbon chain of the production simulation. Solid line, trans; dashed line, gauche$^+$; dotted line, gauche$^-$.

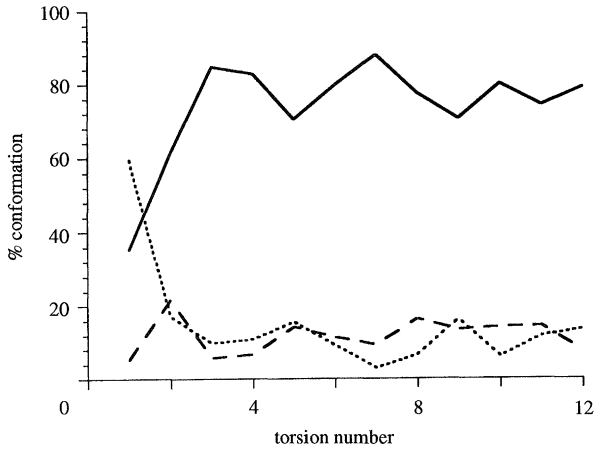

Figure 6. Conformational populations for the S_n2 hydrocarbon chain of the production simulation. Solid line, trans; dashed line, gauche$^+$; dotted line, gauche$^-$.

imprecise for an unambiguous assessment. Furthermore, the oscillations in the profile complicate the analysis. Both the S_n1 and S_n2 hydrocarbon chains have a predominantly gauche conformation at torsion 1, corresponding to the torsion about the C1—C2 bond. However, the gauche$^+$ and gauche$^-$ populations are significantly different for the S_n2 torsion; in relation to this it is worth stating the assertion of Meier *et al.* (1986) that unequal gauche conformations at the C2 methylene of the S_n2 chain are a prerequisite for unequal motional averaging of the two hydrogen atoms at this segment. The simulations seem to support the postulate that the two experimental order parameters of this chain segment arise from different motional averaging. The NMR relaxation study of Mayer *et al.* (1988) suggests that the C2 segment of the S_n2 chain adopts the following conformations at 308 K: trans 8%, gauche$^+$ 68%, gauche$^-$ 24%. Although the simulations support the observation of unequal gauche populations at the C2 segment, the gauche$^-$ conformation is predicted to dominate. Whether this difference is systematic, due to an error in analysing either the simulation or the experimental data, or due to an inconsistency in the dihedral naming procedure, is unknown. However, it is clear that experiment consistently predicts unequal gauche populations at this chain segment, and simulation reproduces this behaviour.

It is possible to determine the correlation times for transgauche isomerization by fitting an exponential function to an angular autocorrelation function. The function adopted was suggested by Levy *et al.* (1979) and is given in equation (6).

$$C(\tau) = < \cos[\phi(t+\tau) - \phi(t)] > . \qquad (6)$$

$C(\tau)$ corresponds to the autocorrelation function at time τ, and ϕ corresponds to the dihedral angle. The average $< \ldots >$ is evaluated over the lipid molecules and simulation time, t. A comment must be made regarding the relation between the correlation times derived from experiment, and the correlation times derived from the function proposed. The NMR correlation times are obtained from relaxation studies, and are therefore related to the behaviour of a second-order Legendre polynomial autocorrelation function, and not the first-order function used above. Furthermore, the NMR correlation times are strictly not equivalent to the correlation times derived from a simple exponential fit to the autocorrelation function (Impey *et al.* 1982); this observation will be considered in more detail in the the section analysing the water dynamics. For example, in the case of deuterium NMR studies of lipid hydrocarbon chains, the deuterium relaxation mechanism is predominantly quadrupolar in nature, and as such relaxation is related to the second-order Legendre polynomial autocorrelation function of the C—D bond vector (Brown *et al.* 1979). It is the correlation time derived from this function that should be related to experiment. Once the validity of the model has been justified on this basis, the behaviour of the dihedral angle autocorrelation function can be studied. Thus whereas the correlation times derived using the autocorrelation function given in equation (6) are of relevance, it is likely that quantitative differences between these values and experiment will occur. A high priority for further work is the monitoring of the autocorrelation function more appropriate to the experimental correlation times.

In table 3, the correlation times derived for each torsion of the hydrocarbon chain by fitting a single exponential function to the autocorrelation function are presented. Two fitting procedures were adopted; the first involved fitting the function to the entire autocorrelation function, and the second involved fitting to just the 21–100 ps section of the curve. In this manner it was hoped to eliminate the effects of fast relaxation at short time, and statistical noise at long time. The caveat given earlier regarding the reliability of simulation correlation times in excess of simulation length also applies here. The R factors derived for the least squares fitting procedure are also presented in table 3. In practice, a straight line was fitted to the natural logarithm of the autocorrelation

Table 3. *Correlation times in ps for trans-gauche isomerization of the hydrocarbon chains*

(Also quoted in parentheses are the R factors derived from the least squares fit.)

torsion number	full fit		21–100 ps fit	
	S_n1	S_n2	S_n1	S_n2
1	237 (0.88)	507 (0.82)	196 (0.99)	430 (0.93)
2	312 (0.94)	183 (0.97)	270 (0.98)	142 (1.00)
3	251 (0.92)	395 (0.87)	228 (0.98)	372 (0.89)
4	168 (0.98)	229 (0.99)	176 (0.99)	271 (0.99)
5	586 (0.67)	284 (0.82)	732 (0.52)	167 (1.00)
6	208 (0.95)	314 (0.95)	185 (0.97)	241 (1.00)
7	212 (0.98)	357 (0.87)	222 (1.00)	352 (0.98)
8	200 (0.85)	408 (0.78)	130 (1.00)	261 (0.96)
9	407 (0.79)	242 (0.92)	291 (0.96)	266 (0.92)
10	202 (0.93)	192 (0.97)	209 (0.90)	168 (0.99)
11	284 (0.98)	190 (0.98)	227 (0.90)	176 (1.00)
12	173 (0.92)	222 (0.95)	163 (0.99)	201 (0.99)

PHILOSOPHICAL TRANSACTIONS OF THE ROYAL SOCIETY B BIOLOGICAL SCIENCES

function. The fit for some of the correlation times is not good, presumably because of the limited data-set size. Clearly, correlation times with R factors any less than 0.9 should be treated with great caution. The two fitting procedures yield results which are broadly similar; the average correlation time for the hydrocarbon torsions is 282 ps for fitting to the full data set, and 253 ps for fitting to the 21–100 ps segment. These values lie at the high end of the experimental range discussed earlier. It is interesting to note that torsion 1 of the S_n2 chain has a longer relaxation time than the equivalent torsion of the S_n1 chain. This is consistent with the S_n2 chain being kinked at the C2 segment for steric packing reasons. It is worth noting that experimentally (Brown *et al.* 1979) the C2 methylene segments of both chains are predicted as having a longer relaxation time than the rest of the methylene groups. However, neither the prediction of a C2–C3 correlation time of 620 ps for the S_n2 hydrocarbon chain (Fuson & Prestegard 1983) nor the mobility gradient is reproduced, although given the statistical uncertainty in the correlation times the latter is not unexpected.

(*b*) *Bilayer dimensions*

If the molecular dynamics simulations are to be regarded as realistic, then they must reproduce the experimentally observed bilayer dimensions, as determined by X-ray and neutron diffraction.

In figure 7, the electron density profile across the bilayer, for the production run, is presented. The bilayer centre is at 0 Å, and was evaluated from the centre of geometry of the lipid molecules. In this manner any membrane drift parallel to the bilayer normal is eliminated from the analysis. The rather crude procedure of assuming atom-centred electron densities without electron reorganization was adopted in the evaluation of this profile; the nitrogen atom was assumed to have a net positive charge, and the phosphorus a net negative charge. This profile does illustrate the experimentally observed behaviour, namely, a pronounced minimum at the bilayer centre, pronounced maxima at the headgroups, and shoulders at the interface of the hydrocarbon region with the headgroups. Visual comparison with the profile for DPPC at 49°C, 8% hydration (Cevc & Marsh 1987), suggests that the hydrocarbon minimum in the simulation profile is too pronounced, although clearly this analysis is subjective.

X-ray scattering experiments (Lewis & Engelman 1983) have been performed on a range of lipids to determine bilayer dimensions; a phosphorus–phosphorus peak spacing of 34 ± 1 Å for DMPC in the L_α phase at 36°C was reported. In figure 8, the phosphorus atom distribution profile along the bilayer normal, derived from the production run, is presented. From this distribution a mean phosphorus–phosphorus distance of 34.6 Å is obtained, in excellent agreement with experiment. However, it is apparent from the distribution that the statistical uncertainty in the simulation value is large; the standard deviation of the phosphorus–phosphorus distance is 4.5 Å. This error was obtained by fitting a Gaussian distribution to the phosphorus atom distribution profile. It is also obvious that the two halves of the bilayer are not equivalent; the distribution on the left (layer 1) is considerably broader than that on the right. Inspection of the simulation coordinates indicates that this effect arises from the presence of a pronounced ripple in layer 1 of the bilayer. This effect is also manifested in the tilt behaviour of the hydrocarbon chains, as described earlier. Whether this pronounced ripple is a real effect, or a simulation artefact, cannot be answered, except that the experimental properties are reproduced despite its presence. Clearly, the rippling may be a physically realistic process, but given the long timescales associated with bulk lipid dynamics, representative sampling of the full ensemble cannot be obtained during the course of what are essentially short simulations. Inspection of the phosphorus–phosphorus distances for the equilibration phase suggests that the bilayer width and associated standard deviation have stabilized after approximately 300 ps.

Neutron diffraction can be used to determine the positions of deuterium atoms within the bilayer with a

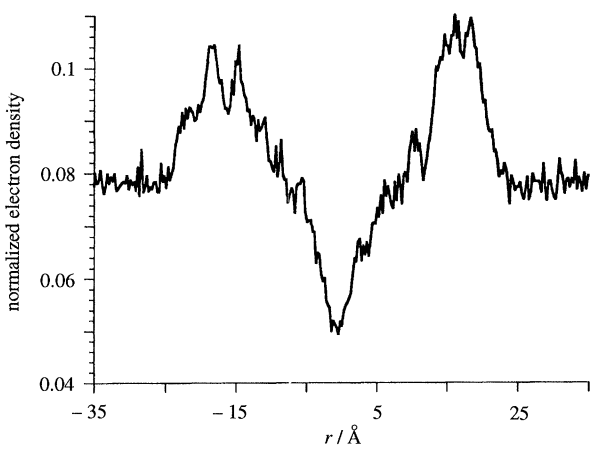

Figure 7. Electron density profile across the lipid bilayer for the production simulation. The electron density is given in arbitrary units.

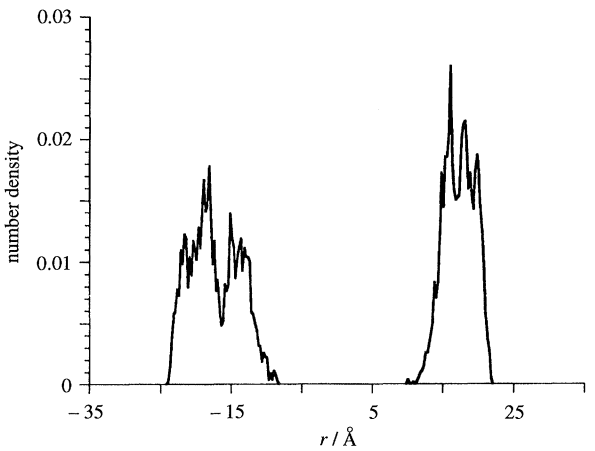

Figure 8. *Z*-axis distribution of phosphorus atoms from the production simulation. Number density is in arbitrary units.

Table 4. *Distances from the bilayer centre for deuterated carbon atoms*

(See table 1 for atom naming convention.)

carbon atom	experiment/Å	modified experiment/Å	simulation/Å
C_α	21.0 ± 1.0	19.5 ± 1.0	17.6 ± 3.2
C_β	21.2 ± 1.0	19.7 ± 1.0	17.8 ± 3.4
C_γ	21.8 ± 0.6	20.3 ± 0.6	18.0 ± 3.5
C	17.4 ± 1.5	15.9 ± 1.5	15.2 ± 3.0
C4	12.2 ± 1.5	10.7 ± 1.5	9.9 ± 3.1
C5	10.5 ± 1.5	9.0 ± 1.5	9.0 ± 3.0
C9 (C7)	8.1 ± 1.0	8.1 ± 1.0	7.3 ± 2.7
C14 (C12)	3.6 ± 1.0	3.6 ± 1.0	3.3 ± 2.6
C15 (C13)	1.9 ± 1.0	1.9 ± 1.0	2.7 ± 2.6

precision of typically less than 1 Å. Büldt *et al.* (1978) have applied the technique to the analysis of DPPC in the L_α phase at 50°C, 25% hydration by mass. The experimental results, together with those obtained from the production simulation, are given in table 4. The standard deviations on the simulation values were obtained by fitting a Gaussian curve to the observed distribution. The interpretation of the data given in table 4 is not trivial. As the lipid used in the experiment contains two extra carbon atoms, compared with the simulation system, a data correction is required. X-ray studies (Lewis & Engelman 1983) give the phosphorus–phosphorus separation for DPPC as 37 ± 1 Å; this is 3 Å larger than this separation in DMPC, and it is therefore reasonable to assume that the hydrocarbon region is 3 Å thicker in DPPC. Therefore, to correct the neutron diffraction results to allow a direct comparison with DMPC, it seems reasonable to subtract 1.5 Å from the experimental values. This has been done in the column labelled 'modified experiment' in table 4. The data for C9, C14 and C15 have been obtained from the equivalent DMPC carbon atoms in the simulation, given in parentheses, and therefore do not require correction. The agreement between theory and experiment is excellent in the hydrocarbon region, especially given the considerable uncertainty in the simulation values. The agreement in the headgroup region is less satisfactory, although the observation that the phosphorus–nitrogen vector is largely parallel to the bilayer surface is reproduced.

These experimental data do not distinguish between the S_n1 and S_n2 hydrocarbon chains. However, inspection of the simulation data indicates that the S_n2 segment is, on average, further from the bilayer centre than the corresponding S_n1 segment. This effect has been probed experimentally using pyrene-labelled phospholipid bilayers (Eklund *et al.* 1992); the S_n1 hydrocarbon chain is observed to penetrate 0.6 ± 0.2 Å further into the hydrocarbon region than the S_n2 chain.

Further neutron diffraction data (Büldt *et al.* 1979; Zaccai *et al.* 1979) have been analysed to give the distribution width of the deuterium atoms within the lipid bilayer, and provide a direct comparison with the simulation standard deviations given in table 4. In table 5, the experimental distribution widths, together with the values obtained from the simulations, are presented. The experimental data were derived for DPPC in the L_α phase at 70°C, with a relative humidity of 10% by mass. This level of hydration is less than that used in the simulations described here, and does raise the possibility that the distribution of the lipid molecules along the bilayer normal could be modified by the relatively close proximity of the headgroups of another bilayer. The experimental data illustrate the increase in distribution width on approaching the bilayer centre, and are consistent with the results of Brownian dynamics (De Loof *et al.* 1991) and statistical mechanical models (Meraldi & Schlitter 1981). However, the current simulation and experiment agree only at C12, and the C_β label is clearly too broadly distributed in the simulations. This may be due to the presence of the bilayer ripple described earlier, or to the difference in timescales between the simulation and experiment. It seems most likely that there is pronounced rippling observed in the bilayer simulation, and that this behaviour is physically unrealistic. The origin of this effect may be the over emphasis of the strength of the water–lipid interactions, encouraging excessive hydration of the glycerol moiety. Alternatively, the simulations may be far too short to sample the full configuration space accessible to the system. Suffice it to say, that the distributions in the headgroup region are too broad, although the behaviour in the bilayer centre is in agreement with experiment.

Table 5. *Experimental and simulation standard deviations of the carbon atom distributions along the bilayer normal*

(The experimental data (Büldt *et al.* 1979; Zaccai *et al.* 1979) are given in terms of υ, the distribution halfwidth at a value of $1/e$. These have been modified to the standard deviation of the Gaussian distribution.)

carbon atom	experiment/Å	simulation/Å
C_β	2.5 ± 0.4	3.4
C4	1.1 ± 0.4	3.1
C9	2.2 ± 0.4	2.7
C12	2.4 ± 0.4	2.6

(*c*) *Polar–apolar interface*

The extent of water penetration into the hydrocarbon region has been determined experimentally using three methods. Firstly, infra-red spectroscopy has been used to show that the carbonyl groups of the glycerol moieties are hydrated; a shift in the C=O stretching frequency is attributed to the presence of hydrogen bonding with water (Fringeli & Günthard 1976; Blume *et al.* 1988). Secondly, neutron diffraction experiments using deuterated water have shown that water penetrates as far as the C=O group of the glycerol moiety (Blechner *et al.* 1990). It has been shown for DPPC in the gel phase that the water concentration is approximately 48% of the bulk at the phosphorus atom. At the C=O group, the amount of

PHILOSOPHICAL TRANSACTIONS OF THE ROYAL SOCIETY B BIOLOGICAL SCIENCES

water was determined as approximately 6% of the maximum. The distribution of water oxygen atoms, the phosphorus atoms, and the carbonyl oxygen atoms as a function of distance along the bilayer normal suggests that the concentration of water at the phosphorus atom is approximately $50 \pm 20\%$ of the bulk concentration, whereas the concentration at the carbonyl oxygen atom is approximately $20 \pm 20\%$ of bulk. The agreement between the neutron diffraction data is excellent at the headgroup, but less satisfactory at the carbonyl group. However, it must be noted that the experiments were conducted on one of the gel phases of DPPC, and therefore the system headgroup surface area is smaller than that of the L_α phase; in DMPC the reduction in headgroup surface area on passing from the liquid crystal to the gel phase (Janiak *et al.* 1979) is of the order of 10 $Å^2$. The error bars given on the simulation water concentrations are derived by determining the water concentration at the mean atom distance $\pm$ its associated standard deviation; they probably constitute an overestimate of the statistical error.

The carbonyl-oxygen water-hydrogen radial distribution functions for the S_n1 and S_n2 hydrocarbon chains are given in figure 9. The radial distribution functions do not approach unity at large distance since they are normalized with respect to the bulk number density of pure water. The figure indicates that water is penetrating into the glycerol region of the bilayer and forming hydrogen bonds with the carbonyl-oxygen, as inferred from infra-red spectroscopy. Integration of the radial distribution functions up to the first minimum indicates that approximately 51% of the S_n1 carbonyl-oxygen atoms and 56% of the S_n2 oxygen atoms are hydrated. This analysis assumes that each oxygen atom is only hydrated by one water-hydrogen atom, and it therefore constitutes an upper limit on the level of hydration. Infra-red studies support the increased hydration of the S_n2 carbonyl oxygen atom (Blume *et al.* 1988); approximately 35% hydration of the carbonyl groups is predicted for DMPC at 30°C. The results therefore suggest that the extent of hydration of the glycerol region is perhaps too large.

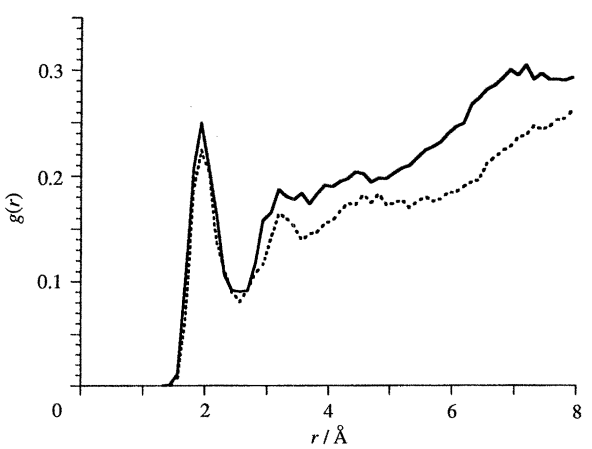

Figure 9. Carbonyl-oxygen and water-hydrogen radial distribution functions for the S_n1 and S_n2 hydrocarbon chains of the production simulation. Solid line, S_n2; dotted line, S_n1.

Inspection of the associated radial distribution functions for the equilibration phase indicate firstly that the starting geometry was over-hydrated, and secondly that the extent of hydration of the carbonyl oxygen atom converged during the final 200 ps of the equilibration phase.

(*d*) *The glycerol moiety*

The conformational behaviour of the glycerol region for a range of lipids has been studied using proton NMR (Hauser *et al.* 1988). The results for DPPC at 25°C under non-aqueous conditions suggest that the dihedral angles θ_3 and θ_4, defined in figure 1, adopt three conformations (A, B and C) with the populations specified in table 6. Furthermore, studies on a range of phospholipids suggest that most molecules primarily adopt conformations A and B in both solution and micelles. This observation should be confirmed by the simulations, if the behaviour of the glycerol region is reliable. Also presented in table 6 are the conformational populations of θ_3 and θ_4 derived from the production and equilibration simulations. It is clear that the simulations conform to the predictions of the NMR data, and furthermore that only conformations A and B are adopted. Moreover, the conformational behaviour of the glycerol moiety appears stable after 300 ps of simulation.

Other NMR experiments (Strenk *et al.* 1985) on DMPC at 30°C suggest that the glycerol backbone region of the lipid, including the C2 segment of the S_n1 hydrocarbon chain, is rigid on the NMR timescale, and that the glycerol conformations adopted are almost identical to those of conformer B in the DMPC crystal structure (Pearson & Pascher 1979). There is a significant correlation between the crystal structure angles, and the populations derived from the simulation; the behaviour of β_4 shows the worst agreement, although as this dihedral angle is part of the hydrocarbon chain and remote from the glycerol region, this observation is not surprising. However, the glycerol backbone is definitely not rigid on the simulation timescale, supporting the experimental analysis of Hauser *et al.* (1988).

(*e*) *The headgroups*

The behaviour of the lipid headgroups is likely to be very important in terms of moderating the effect of bilayer hydration, and also in terms of the interaction of a charged solute with the bilayer. Furthermore, the electrostatic interactions between the lipid headgroups are critical in determining the observed surface area. Thus it is important that the observed headgroup behaviour reproduces that predicted from experimental data. In figure 1, the relevant dihedral angles which will be discussed in this section are shown.

In table 7, the conformation populations of the headgroup dihedral angles are presented for the production simulation. There is little experimental

PHILOSOPHICAL TRANSACTIONS OF THE ROYAL SOCIETY B BIOLOGICAL SCIENCES

Table 6. *Percentage NMR populations of glycerol torsions* θ_3 *and* θ_4

(The conformations A, B and C are defined in terms of the values of θ_3 and θ_4, in that order. Both simulation and experimental results are presented.)

simulation/experimental observation	A, t, g^+	B, g^+, g^-	C, g^-, t
DPPC, 25°C, in chloroform/methanol	52.0	40.0	7.5
equilibrium simulation, 0–100 ps	96.5	3.5	0.0
equilibration simulation, 100–200 ps	94.4	5.6	0.0
equilibration simulation, 200–300 ps	92.9	7.1	0.0
equilibration simulation, 300–400 ps	86.9	13.1	0.0
production simulation	86.8	13.2	0.0

data available for the conformation populations of these torsions in isolation; the data tend to be interpreted in terms of a sequence of torsional angles. However, Raman spectroscopy (Akutsu 1981) suggests that α_5 should be predominantly gauche. This is clearly not reproduced by the simulations, presumably because of the very crude parameter set selected; no effort was made to parameterize either the headgroup electrostatics, or the dihedral energy terms, both of which critically determine conformation populations. Thus the simulations are clearly inadequate at reproducing this particular headgroup conformation. Also presented in table 7 are the conformations observed in the X-ray study of crystalline DMPC (Pearson & Pascher 1979). There is a remarkable correlation between the crystal angles and the simulation populations for all torsions except α_5. This further supports the assertion that the simulation behaviour of α_5 is physically unrealistic.

Seelig *et al.* (1977) have performed a phosphorus-31 and deuterium NMR study on DPPC bilayers in the liquid crystalline phase which suggests that the headgroups exhibit restricted motion consistent with the rapid transition between two symmetry related conformations. The angles of α_1–α_5 predicted by this work are 170°, −60°, −64°, −145° and 81°, respectively, together with the corresponding negative angles. These results are similar to the crystallographic angles given in table 7. The simulations do not show any appreciable population of these conformational series, as α_5 is almost never gauche. However, the sum of the populations of t, g^+, g^+, t, t and t, g^-, g^-, t, t (α_1–α_5) is 23.6%, suggesting that, with the exception of α_5, the analysis of Seelig *et al.* (1977) is supported.

Skarjune & Oldfield (1979) have also performed phosphorus-31 and deuterium NMR studies on phospholipids. However, this paper asserts that the NMR data are insufficient to obtain a unique set of conformation angles, but that instead only a range of conformation angles can be assigned to each torsion. With this in mind the broad distribution of dihedral angle populations given in table 7 appears justified.

Phosphorus-31 NMR relaxation studies (Dufourc *et al.* 1992) have been used to determine the correlation times for motion about α_2, α_1 and θ_1. The simulation correlation times derived from fitting the first-order Legendre polynomial autocorrelation function (equation (6)) for these dihedral angles with a single exponential curve, are presented in table 8 together with the NMR data. However, only the data for α_2 are derived for the system in the L_α phase; it is unclear whether α_1 and α_1 are undergoing free rotation or librational motion in this phase. A range of values are quoted for the experimental correlation times, illustrating the temperature dependence of these results. The agreement between simulation and experiment is excellent for α_2 although the caveats given earlier regarding the equivalence of NMR and simulation correlation times apply here. Thus the comparison between simulation and experiment should only be treated in terms of an order of magnitude estimate. With this in mind, the agreement for α_2 is gratifying.

The measurement of dielectric properties of phospholipids allows for the direct determination of relaxation times for the headgroup dipole moment. Experiment suggests that the DPPC phospholipid dipoles lie in the plane of the bilayer (Shepherd & Büldt 1978), in agreement with neutron diffraction studies. Furthermore, the dielectric relaxation time was determined as 2.3 ns at 50°C, 25% water by mass. In figure 10 the total lipid dipole moment per

Table 7. *Headgroup conformation populations for the production simulation, together with the dihedral angles observed for the two molecules in the asymmetric unit of the crystal structure of DMPC (Pearson & Pascher 1979)*

	simulation populations			crystallographic angles	
dihedral angle	trans	$gauche^+$	$guache^-$	A	B
α_1	66.1	9.8	24.1	162	170
α_2	18.6	45.1	36.3	68	−76
α_3	21.6	40.3	38.1	63	−46
α_4	75.6	12.2	12.2	139	−161
α_5	91.0	5.7	3.3	−51	64

PHILOSOPHICAL TRANSACTIONS OF THE ROYAL SOCIETY B BIOLOGICAL SCIENCES

Table 8. *Correlation times, in ps, for the indicated dihedral angles derived from fitting a single exponential to the associated autocorrelation function*

(The experimental correlation times for α_1 and θ_1 were obtained using a graph in the source paper (Dufourc *et al.* 1992), and correspond to the lipid system in the $P_{\beta'}$ phase at a temperature of approximately 300 K.)

dihedral	full fit	21–100 ps fit	experiment
α_1	434 (0.96)	404 (0.98)	$\tau > 1000$
α_2	393 (0.94)	336 (0.95)	$400 < \tau < 700$
θ_1	1275 (0.96)	2134 (0.99)	$\tau > 3000$

molecule is presented for layer 1 of the lipid bilayer as a function of time for the production simulation; similar behaviour is observed for layer 2. The figure clearly shows that the net z component of the dipole moment is virtually zero, consistent with the experimental observation that the mean dipole moment lies parallel to the bilayer surface.

The magnitude of the net dipole moment in each half of the lipid bilayer is small, indicating that the dipole moments are arranged in either a predominantly antiparallel or random fashion. Inspection of the individual lipid dipole moments does indicate that the antiparallel arrangement of the starting geometry is largely conserved in the production simulation, although the pronounced bilayer ripple renders this assertion very subjective. In the crystalline starting geometry, the dipole moments are aligned in a predominantly antiparallel arrangement along the y axis. It is interesting to note that layer 1 of the bilayer appears to have a larger average dipole moment than layer 2; whether this is a consequence of the presence of the pronounced ripple in layer 1, an acceptable fluctuation, or a systematic change from the parallel to antiparallel dipole moment arrangement, is unknown.

The timescale over which the molecular dipole moment rotates can be examined by evaluating the appropriate autocorrelation function, given in equation (7). The individual cartesian components of the dipole moments can also be monitored in an analogous manner.

$$C(\tau) = < \mu_i(t)\mu_i(t+\tau) > . \quad (7)$$

$\mu_i(t)$ and $\mu_i(t+\tau)$ correspond to the dipole moments of molecule i at times t and $t+\tau$. In table 9, the correlation times derived from fitting an exponential to these functions are presented. The figures in parentheses correspond to the correlation coefficients obtained from the fitting procedure. Two fitting procedures were adopted; the first involved fitting to the entire autocorrelation function, and the second to just the 21–100 ps section of the function. Also presented in table 9 are the correlation times derived from fitting to the autocorrelation function for just the headgroups, i.e. the charges associated with the ester groups are omitted. The correlation time derived from the dipole moments of each lipid molecule is of the order of 800 ps, and as such it is not surprising that the antiparallel arrangement of the dipole moments present in the starting geometry is conserved in the production simulation. The comparatively short value of the z component suggests that the observation of the lipid dipole moments parallel to the bilayer surface is a real effect, and not an artefact of the starting geometry. As previously stated, correlation times in excess of the length of simulation can only be regarded as estimates. However, the data suggest that simulations in excess of 1 ns are needed to ensure equilibration of the headgroup region.

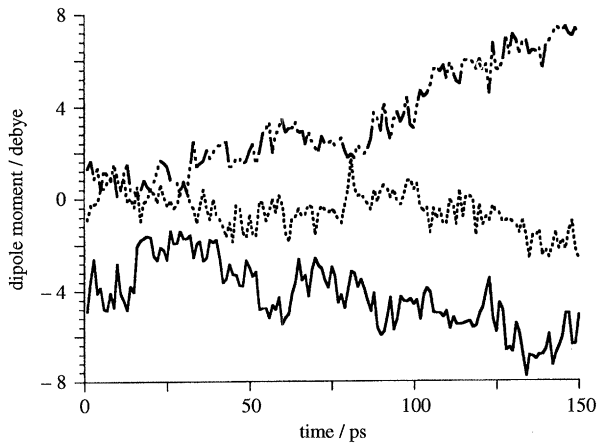

Figure 10. Net dipole moment for layer 1 of the lipid bilayer. Solid line, x; dot-dashed line, y; dotted line, z.

(*f*) *Water behaviour*

In figure 11, the one-dimensional diffusion coefficients for the water molecules are presented as a function of distance from the bilayer centre. The plot was derived by placing each water molecule in a given layer according to its distance from the bilayer centre; each layer was selected to be 2 Å wide. The distance each molecule diffuses in the x, y and z directions in the course of 1 ps was then evaluated, and the resulting displacement distribution fitted to a Gaussian function. The standard deviation of the Gaussian, s, was used in conjunction with equation (8) to obtain an estimate of the diffusion coefficient in that dimension (Raghavan *et al.* 1992).

$$\sigma^2 = 2D\Delta t. \quad (8)$$

D corresponds to the diffusion coefficient, and Δt to the time step over which the displacement function was evaluated. This is merely the one-dimensional Einstein equation. A consequence of this method is that the diffusion of a particle within a given layer is ascribed to that layer, regardless of whether it is still in the layer after time Δt. This serves to place a limit on the value of Δt that can be used; if Δt is too large, then any diffusion gradient observed on approaching the lipid headgroups from the bulk water phase will be reduced. In figure 11, only those water layers with greater than 1000 data sets are presented, corresponding to an average of at least 6.7 water molecules per layer. The choice of 1 ps for Δt will result in the diffusion coefficient estimate being too large; this is

PHILOSOPHICAL TRANSACTIONS OF THE ROYAL SOCIETY B BIOLOGICAL SCIENCES

Table 9. *Correlation times in ps derived by fitting a single exponential to the dipole moment autocorrelation function*
(The figures in parentheses represent the correlation coefficients obtained from the fitting procedure.)

	full dipole moment		headgroup dipole moment	
dipole moment	full fit	21–100 ps fit	full fit	21–100 ps fit
total	804 (0.98)	836 (1.00)	798 (0.98)	816 (1.00)
x	715 (0.88)	797 (0.93)	743 (0.87)	788 (0.93)
y	1202 (0.98)	1261 (0.96)	1197 (0.98)	1255 (0.96)
z	187 (0.97)	175 (1.00)	165 (0.97)	154 (1.00)

because equation (8) is, strictly speaking, only valid at long times, as the oscillations of a molecule about some mean position will contribute to the diffusion coefficient if Δt is small. This will be particularly true for water molecules bound to the lipid headgroups. However, the accumulation of the displacement distribution for each layer involves the use of a histogram, and therefore underestimates the diffusion coefficient. Simulations on pure TIP3P water suggest that the use of equation (8) underestimates the diffusion coefficient by 10%, as compared to the diffusion coefficient obtained using the Einstein equation with large Δt.

The data presented in figure 11 illustrate a number of interesting points. Firstly, the water diffusion coefficient decreases on approaching the polar headgroups; this is as expected. A region of fast water diffusion between the bulk water phase and that bound by the charged headgroups is observed. There does not appear to be a reduction in water density at this point, although this analysis is complicated by the presence of the headgroups. Furthermore, the diffusion gradient is less marked on the left of the bilayer (layer 1), consistent with the greater width of the headgroup region in this half, as described earlier.

Figure 11 also shows that the perturbing effect of the charged headgroups extends approximately 15 Å into the aqueous layer. The correlation length of the aqueous phase corresponds to the characteristic length of the solvent structure. Strictly speaking, it is the decay constant determined from fitting an exponential function to the property in question; this procedure is difficult to perform for the diffusion coefficient profile. Quantitative estimates of the correlation length span a considerable range (Cevc & Marsh 1987). Hydration force measurements with mica plates suggest a value of 10 Å; X-ray diffraction studies suggest a value of between 1.4 Å and 3.2 Å, with an average of 2.5 Å, and water vapour adsorption isotherms yield values of between 0.8 Å and 1.3 Å. Thus the value obtained from the simulations on the basis of the diffusion coefficient behaviour is, at least, of the correct order of magnitude, although larger than expected from experiment. It should be borne in mind that the various experimental techniques are sensitive to different solvent properties. The simulation value is also likely to be very dependent on the choice of non-bonded cutoff, and on the treatment of long-range electrostatic interactions (Alper *et al.* 1993). However, the observation of correlations in the water structure over distances in excess of 8 Å does suggest that the influence of the headgroups on the water behaviour is propagated by waterwater interactions.

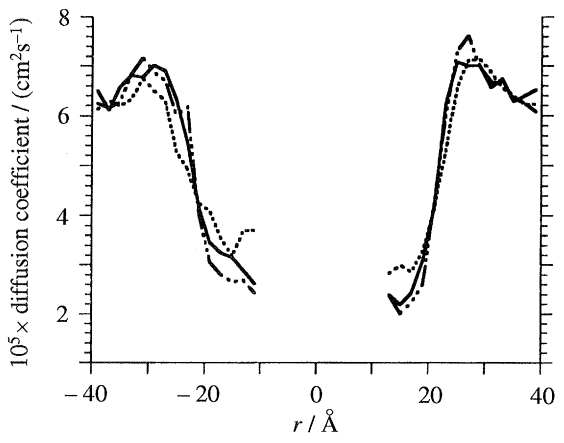

Figure 11. One-dimensional diffusion coefficients for the water molecules as a function of distance from the bilayer centre. Bilayer centre is set at the origin. Solid line, *x*; dot-dashed line, *y*; dotted line, *z*.

The available experimental data on water diffusion in lipid systems are extensive. Radioactive studies using tritium-doped water molecules on lecithin at 22°C have obtained a water diffusion profile as a function of the percentage of water in the system (Rigaud *et al.* 1972). The percentage of water has been interpreted in terms of the thickness of the aqueous region between separate bilayers. The experimental data indicate that a diffusion coefficient of 0.1×10^{-5} $cm^2 s^{-1}$ is observed for an aqueous layer width of 17 Å, increasing to values of greater than 1.0×10^{-5} $cm^2 s^{-1}$ for aqueous layer widths of greater than 33 Å.

In comparing these data with those obtained from the simulations a number of points must be considered. Firstly, simulation and experiment are carried out at different temperatures, and therefore a direct quantitative comparison is difficult; the Stokes-Einstein equation suggests that the simulation diffusion coefficients should be approximately 10% larger than the experimental values. Secondly, the experimental diffusion coefficient gradient is not obtained as a function of distance from the headgroups in a fully hydrated system. Instead, the percentage water present is modified, and the associated diffusion coefficient monitored. Thus changes in the bilayer structure associated with increasing the extent of hydration are bound to influence the data. In

conclusion, the experimental data are unsatisfactory for the purpose of making a direct quantitative comparison with the simulation results. However, the data illustrate the presence of a diffusion gradient associated with the extent of water binding to the charged headgroups. Furthermore, the experimental data suggest that the water molecules in the vicinity of the charged headgroups have diffusion coefficients of the order of one third to one tenth the value in the bulk phase, and this is reproduced in the simulations.

Further NMR studies (Klose & Gawrisch 1981) also give a diffusion coefficient gradient; free water is given a value of $10^{-5}\,\mathrm{cm^2\,s^{-1}}$, and water in the main hydration shell a value of $2 \times 10^{-9}\,\mathrm{cm^2\,s^{-1}}$. However, this paper does not detail the experimental conditions, nor the precise lipid molecules used. Thus the direct quantitative comparison between experiment and simulation is problematic, but the presence of a diffusion gradient is consistent to both.

In figure 12 the water order parameters defined in terms of the angle between the O—H bond vector and the bilayer normal, in conjunction with equation (2), are presented. The water molecules were assigned to 2 Å thick layers, and any layer in which less than 1000 data sets were averaged was eliminated. This figure clearly shows that the water molecules are not tumbling isotropically in the vicinity of the polar headgroups; this is as expected. Furthermore, the influence of the headgroups extends into the water layer a distance of approximately 10 Å, although the correlation length determined by the approximate fitting of an exponential function to the order parameter profile is of the order of 3 Å. This is in agreement with the experimental data reported earlier. Similar order parameter behaviour has been reported in Monte Carlo simulations using fixed lipid molecules and TIPS2 water (Scott 1984). In this study, the lipid molecules were fixed with their headgroups either parallel or antiparallel, and the associated order parameters for the water layer nearest the headgroups were 0.13 ± 0.02 and 0.08 ± 0.03, respectively. The authors are not aware of any direct experimental values for the water order parameters. However, quadrupolar splitting values obtained from deuterium NMR using heavy water in conjunction with egg yolk lecithin (Finer 1973), suggest increased orientational ordering in water molecules bound to the lipid headgroups, in agreement with simulation.

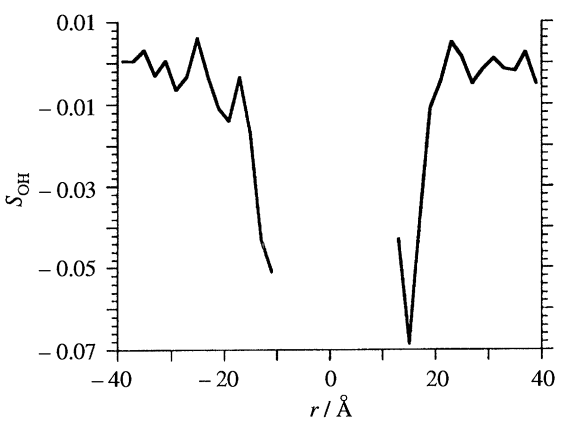

Figure 12. Water order parameters as a function of distance from the bilayer centre.

The orientational behaviour of the water molecules can be studied experimentally using NMR relaxation studies; qualitatively, one would expect the rate of orientational averaging of the water molecules to be reduced on approaching the charged lipid bilayer surface. The time dependent orientational behaviour of water molecules in the simulations can be probed be evaluating the angular autocorrelation function (Madden & Impey 1986), $C_1^z(t)$, given in equation (9).

$$C_1^z(t) = < P_1\,[{}^1e_z(t) \cdot {}^1e_z(0)] > . \qquad (9)$$

P_1 is a Legendre polynomial of rank l, and ${}^1e_z$ a unit vector pointing along the zth direction in the molecular frame of reference. In the work that follows, the z direction corresponds to the inter-hydrogen vector of the water molecules, the y direction to the water dipole moment vector, and the x direction to the vector perpendicular to z and y. The full orientational correlation function described in equation (9) can be fitted to a rapidly decaying oscillatory function, and comparatively long-lived exponential function, thus:

$$C_1^z(t) = \phi_1^z(t) + A_1^z \exp(-t/\tau_1^z). \qquad (10)$$

The rapidly oscillating function corresponds to the fast librational motion of the water molecules, and this decays away within about 0.2 ps. NMR correlation times can be obtained by analysis of the correlation function derived for the second order Legendre polynomial given in equation (11).

$$P_2[x] = 0.5(3x^2 - 1). \qquad (11)$$

The correlation times derived from the associated autocorrelation functions can then be interpreted in terms of the observed NMR correlation times. The final 20 ps of the production simulation was analysed, the coordinate sets being separated by 0.2 ps. For this reason the characteristic 'glitch' associated with the fast librational motion is not observed.

NMR analyses of water dynamics allow for a comparison between simulation and experiment to be made. The reorientational correlation times as derived from T_1 NMR studies can be estimated (Impey *et al.* 1982) using the result given in equation (12).

$$\tau_{\mathrm{NMR}} = A_2^z\,\tau_2^z. \qquad (12)$$

The quantity τ_{NMR} corresponds to the correlation time associated with intramolecular dipoledipole relaxation. In figure 13, the quantity τ_{NMR} is presented for the autocorrelation functions derived using the molecular z axis (the interproton vector) and also the OH bond vectors. The figure illustrates the difference in behaviour observed in the two halves of the lipid bilayer. The correlation time for the bulk phase is approximately 0.6 ps, whereas water molecules bound to the headgroups show a correlation time of approximately 2.5 ps. The behaviour of the two halves of the bilayer in the vicinity of the headgroups is considerably different, presumably

PHILOSOPHICAL TRANSACTIONS OF THE ROYAL SOCIETY B BIOLOGICAL SCIENCES

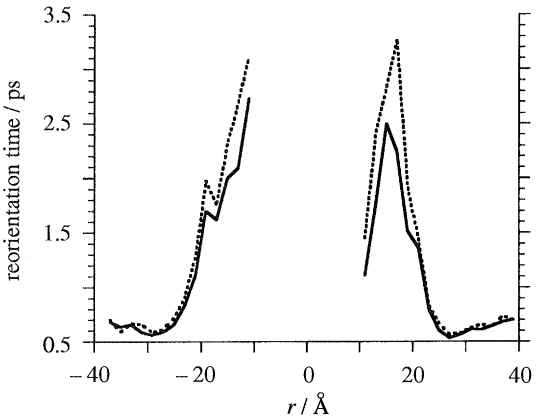

Figure 13. τ_{NMR} derived using equation (12) for the interproton vector and the OH bond vector of the water molecules. Dotted line, *z*; solid line, OH.

owing to the pronounced rippling of layer 1. The experimental values (Jonas *et al.* 1976) for τ_{NMR} for water are 2.07 ps at 30°C, and 0.85 ps at 90°C; thus the simulation value for free water is too small. However, other simulation results are also too small (Impey *et al.* 1982); a value of 0.6 ps was obtained at 87°C using the MCY water model. The simulations of Madden & Impey (1986), give τ_{NMR} for water in the first coordination shell of a lithium ion as 5.8 ps at 297 K, 2.9 times smaller than the equivalent pure water correlation time. The ratio for the larger K^+ ion is unity, a considerable reduction. On this basis, binding to ions is expected to increase the value of τ_{NMR} by at most a factor of approximately 3. The lipid simulation results support this increase in τ_{NMR} on binding to the charged headgroups.

There are experimental data available for the reorientational correlation time for heavy water in a hydrated membrane system, derived from an analysis of the T_1 and T_2 relaxation times (Finer 1973). The experimental data give a correlation time of 3 ps for bulk water, increasing to 1×10^5 ps for tightly bound water. In the simulations described here, all water molecule types should be present. The experimental increase in correlation time on water binding to the lipid headgroups is significantly greater than that observed in the simulations. Because the primary relaxation process is quadrupolar in nature, the second-order Legendre polynomial autocorrelation function of the electric field gradient tensor at the hydrogen nucleus should be evaluated if a direct comparison with this experiment is to be made. However, it appears to be an acceptable approximation to reduce the behaviour of the electric field gradient tensor to that of the OH bond vector (Finer 1973), and thus the OH correlation times given in figure 13 are the appropriate simulation values for comparison with the experimental data. The difference between simulation and experiment is marked. However, a number of points do require discussion.

The NMR data only provide an upper limit to the correlation times. Furthermore, the experiments were performed using heavy water at presumably 23°C, whereas the simulations used conventional water at 50°C. Thus the experimental correlation times should be larger than their simulation counterparts. Furthermore, the experimental data were obtained by changing the water content of the sample, and consequently the low hydration limit data are likely to be substantially affected by the presence of neighbouring bilayers. Thus the applicability of the experimental data as a measure of simulation reliability is questionable.

(*g*) *Diffusion behaviour*

In figure 14, the square of the displacement behaviour of the branching carbon atom in the glycerol moiety, atom 5 in figure 1, together with the diffusion coefficient, are presented as a function of simulation time for the production run. Two sets of data are presented; one corresponds to the three-dimensional displacement data, and the associated diffusion coefficient evaluated using the Einstein equation. The second set of data corresponds to the two-dimensional displacement data evaluated using the *x* and *y* coordinates of the carbon atom, thereby excluding motion parallel to the bilayer normal, together with the associated diffusion coefficient. The Einstein equation in two dimensions is given in equation (13).

$$D = (1/4t) < |r(t) - r(0)|^2 > . \qquad (13)$$

$r(t) - r(0)$ is the two-dimensional displacement vector. The first 9 ps of the production simulation time were not used. Furthermore, to improve the statistics, the time zero was reset to the succeeding coordinate set from 10 ps to 30 ps into the simulation. Thus the data presented in figure 14 are actually an average over 21 analyses, with time origins of 10 ps, 11 ps, 12 ps . . . 30 ps. This should improve the otherwise poor statistics which arise from the very small number of lipid molecules in the simulation system. However, the successive time origins are highly correlated, and thus

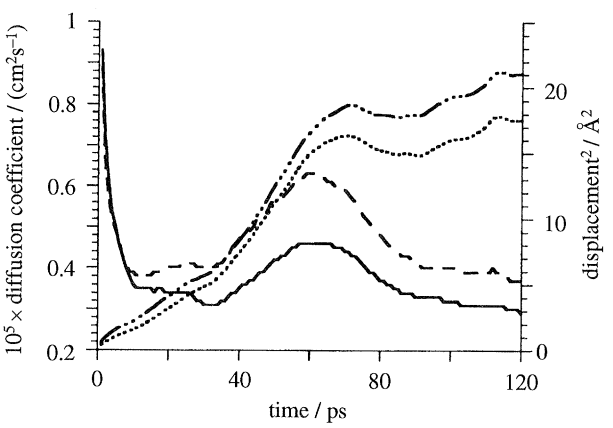

Figure 14. The square of the displacement and corresponding diffusion coefficient for the lipid molecules in the production simulation. Two sets of data corresponding to the two-dimensional and three-dimensional diffusion coefficients are presented. Solid line, three-dimensional diffusion coefficient; dashed line, two-dimensional diffusion coefficient; dot-dashed line, three-dimensional displacement; dotted line two-dimensional displacement.

PHILOSOPHICAL TRANSACTIONS OF THE ROYAL SOCIETY B BIOLOGICAL SCIENCES

the convergence behaviour is still likely to be poor. The observed diffusion coefficients are approximately $0.3 \times 10^{-5}\,cm^2\,s^{-1}$ and $0.4 \times 10^{-5}\,cm^2\,s^{-1}$ for the three-dimensional and two-dimensional analyses, respectively. The two-dimensional diffusion coefficient is larger than the three-dimensional value suggesting that the diffusive motion in the direction of the bilayer normal is very limited. Furthermore, this suggests that the pronounced rippling reported earlier is long lived. However, since the mean lipid displacement is significantly less than half the simulation system dimensions, the reliability of the diffusion coefficients is poor. The system geometry is such that the two-dimensional diffusion coefficient is appropriate for comparison with experiment.

The experimental values for the lipid diffusion coefficient range from 10^{-7} to $10^{-8}\,cm^2\,s^{-1}$, depending on the method selected (Small 1986), although the majority of results are of the order of $10^{-8}\,cm^2\,s^{-1}$. For example, Rommel *et al.* (1988) quote a value derived from NMR relaxation studies on DMPC at 303 K of $3 \times 10^{-8}\,cm^2\,s^{-1}$.

Despite the broad range of experimental values for the lipid diffusion coefficients, the simulation results give a diffusion coefficient which is at least one order of magnitude too large. A possible explanation is that the simulations are too short to obtain a reliable estimate of what is essentially a slow process. The pronounced nonlinear behaviour observed in the displacement graphs also suggests inadequate convergence.

4. SUMMARY AND CONCLUSION

In this paper, a 550 ps molecular dynamics simulation of the phospholipid DMPC has been reported. Extensive comparison of the simulation behaviour with the available experimental data suggest that the simulation is physically realistic.

The order parameters of the hydrocarbon region show good agreement with experiment, as do the bulk conformation populations. It is apparent that simulations within a rigid water matrix are inadequate at reproducing the behaviour of the hydrocarbon region, and therefore this procedure cannot be recommended as a method of improving computational efficiency. It is interesting to note that the observation of an unequal gauche$^+$–gauche$^-$ population in the first dihedral angle of the S_n2 chain supports the hypothesis that the two experimental C2, S_n2 order parameters arise from unequal motional averaging at this chain segment. The cistrans isomerization correlation times observed from the trajectory are broadly consistent with the experimental data, although the mobility gradient predicted from NMR is not reproduced. Inspection of the tilt behaviour of the hydrocarbon region suggests that although the timescale over which chain motion occurs is realistic, the simulation system is too small, and the simulation too short.

The bilayer dimensions and mean position of atoms with respect to the bilayer centre are in good agreement with X-ray and neutron diffraction data. The simulation does, however, show a pronounced ripple which renders the width of the headgroup distribution too large. Whether this is a consequence of the parameter set, a simulation artefact arising from the size and implementation of the non-bonded cutoff, or a physically realistic fluctuation in the course of what is a short simulation on the experimental timescale, is unknown.

The carbonyl groups of the glycerol region are observed to be hydrated, as predicted by experiment, and the conformational behaviour of the glycerol region is also consistent with experiment.

The conformational behaviour of the headgroups is incorrect at α_5, although the remainder of the headgroup dihedrals appear to be in agreement with NMR analyses. Presumably, more careful parameterization of the headgroup region is required to eliminate this error. The headgroups are observed to lie, on average, in the plane of the bilayer. However, the magnitude of the correlation times suggest that simulations in excess of 1 ns are needed to reliably equilibrate the headgroup region.

The water molecules above the membrane exhibit diffusion gradients, orientational polarization, and rotational correlation times consistent with experiment. However, the lipid molecules have diffusion coefficients that are at least one order of magnitude too large, although the simulation results are not reliably converged.

The level of agreement between simulation and experiment is very promising, although clearly a number of points require further study. Longer simulations on larger systems need to be performed to determine the consistency of the results. The inclusion of long-range electrostatic interactions, a larger non-bonded cutoff, and an explicit treatment of polarization also need to be addressed. However, given the crude nature of the parameterization and simulation protocol, the observed agreement between simulation and experiment is very satisfactory. The results suggest that this membrane model is broadly reliable, and can therefore be used in more complex, multiple component simulations.

J.W.E. acknowledges the generous support of Glaxo Group Research in the form of a Glaxo Research Scholarship. We thank CRAY Research U.K. for a generous grant of computer time on their CRAY X-MP at Bracknell, and Pearson & Pascher (1979) for providing the coordinates of the crystal structure of DMPC.

REFERENCES

Akutsu, H. 1981 Direct determination by Raman scattering of the conformation of the choline group in phospholipid bilayers. *Biochemistry* **20**, 7359–7366.

Allen, M.P. & Tildesley, D.J. 1987 *Computer simulation of liquids*. Oxford University Press.

Alper, H.E., Bassolino, D. & Stouch, T.R. 1993 Computer simulation of a phospholipid monolayer-water system: the influence of long range forces on water structure and dynamics. *J. chem. Phys.* **98**, 9798–9807.

Alper, H.E. & Levy, R.M. 1989 Computer simulations of the dielectric properties of water: studies of the simple

PHILOSOPHICAL TRANSACTIONS OF THE ROYAL SOCIETY B BIOLOGICAL SCIENCES

point charge and transferrable intermolecular potential models. *J. chem. Phys.* **91**, 1242–1251.

Berendsen, H.J.C., Postma, J.P.M., van Gunsteren, W.F., DiNola, A. & Haak, J.R. 1984 Molecular dynamics with coupling to an external bath. *J. chem. Phys.* **81**, 3684–3690.

Berkowitz, M.L. & Raghavan, K. 1991 Computer simulation of a water/membrane interface. *Langmuir* **7**, 1042–1044.

Blechner, S.L., Skita, V. & Rhodes, D.G. 1990 Structure of polymerisable lipid bilayers: water profile of a diacetylenic lipid bilayer using elastic neutron scattering. *Biochim. biophys. Acta* **1022**, 291–295.

Blume, A., Hübner, W. & Messner, G. 1988 Fourier transform infrared spectroscopy of $^{13}C=O$ labelled phospholipids. Hydrogen bonding to carbonyl groups. *Biochemistry* **27**, 8239–8249.

Brown, M.F., Seelig, J. & Häberlen, U. 1979 Structural dynamics in phospholipid bilayers from deuterium spin-lattice relaxation time measurements. *J. chem. Phys.* **70**, 5045–5053.

Büldt, G., Gally, H.U., Seelig, A., Seelig, J. & Zaccai, G. 1978 Neutron diffraction studies on selectively deuterated phospholipid bilayers. *Nature, Lond.* **271**, 182–184.

Büldt, G., Gally, H.U., Seelig, J. & Zaccai, G. 1979 Neutron diffraction studies on phosphatidylcholine model membranes. I. Head group conformation. *J. molec. Biol.* **134**, 673–691.

Cevc, G. & Marsh, D. 1987 *Phospholipid bilayers. Physical principles and models*. New York: John Wiley & Sons.

Charifson, P.S., Hiskey, R.G. & Pederson, L.G. 1990 Construction and molecular modelling of phospholipid surfaces. *J. comput. Chem.* **11**, 1181–1186.

Chirlian, L.E. & Francl, M.M. 1987 Atomic charges derived from electrostatic potentials: a detailed study. *J. comput. Chem.* **8**, 894–905.

Damodaran, K.V. & Merz, K.M. 1993 Head group-water interactions in lipid bilayers: a comparison between DMPC- and DLPE-based lipid bilayers. *Langmuir* **9**, 1179–1183.

Damodaran, K.V., Merz, K.M. & Gaber, P.B. 1992 Structure and dynamics of the dilauroylphosphatidylethanolamine lipid bilayer. *Biochemistry* **31**, 7656–7664.

Davis, J.H. 1979 Deuterium magnetic resonance study of the gel and liquid crystalline phases of dipalmitoyl phosphatidylcholine. *Biophys. J.* **27**, 339–358.

Davis, J.H. 1983 The description of membrane lipid conformation, order and dynamics by ^{2}H-NMR. *Biochim. biophys. Acta* **737**, 117–171.

De Loof, H., Harvey, S.C., Segrest, J.P. & Pastor, R.W. 1991 Mean field stochastic boundary molecular dynamics simulation of a phospholipid in a membrane. *Biochemistry* **30**, 2099–2113.

De Young, L.R. & Dill, K.A. 1988 Solute partitioning into lipid bilayer membranes. *Biochemistry* **27**, 5281–5289.

Dufourc, E.J., Mayer, C., Stohrer, J., Althoff, G. & Kothe, G. 1992 Dynamics of phosphate head groups in biomembranes. Comprehensive analysis using phosphorus-31 nuclear magnetic resonance lineshape and relaxation time measurements. *Biophys. J.* **61**, 4257.

Edholm, O. & Nyberg, A.M. 1992 Cholesterol in model membranes. A molecular dynamics simulation. *Biophys. J.* **63**, 1081–1089.

Egberts, E. 1988 Molecular dynamics simulation of multibilayer membranes. Ph.D. thesis, University of Groningen, The Netherlands.

Egberts, E. & Berendsen, H.J.C. 1988 Molecular dynamics simulation of a smectic liquid crystal with atomic detail. *J. chem. Phys.* **89**, 3718–3732.

Eklund, K.K., Virtanen, J.A., Kinnunen, P.K.J., Kasurinen, J. & Somerharju, P.J. 1992 Conformation of phosphatidylcholine in neat and cholesterol-containing liquid-crystalline bilayers. Application of a novel method. *Biochemistry* **31**, 8560–8565.

Engel, A.K. & Cowburn, D. 1981 The origin of multiple quadrupole couplings in the deuterium NMR spectra of the 2 chain of 1,2 dipalmitoyl-sn-glycero-3-phosphorylcholine. *FEBS Lett.* **126**, 169–171.

Finer, E.G. 1973 Interpretation of deuteron magnetic resonance spectroscopic studies of the hydration of macromolecules. *J. chem. Soc., Faraday Trans. 2* **69**, 1590–1600.

Fringeli, U.P. & Günthard, H.H. 1976 Hydration sites of egg phosphatidylcholine determined by means of modulated excitation infrared spectroscopy. *Biochim. biophys. Acta* **450**, 101–106.

Fuson, M.M. & Prestegard, J.H. 1983 Dynamics of an interfacial methylene in dimyristoylphosphatidylcholine vesicles using carbon-13 spin relaxation. *Biochemistry* **22**, 1311–1316.

Hauser, H., Pascher, I. & Sundell, S. 1988 Preferred conformation and dynamics of the glycerol backbone in phospholipids. An NMR and X-ray single-crystal analysis. *Biochemistry* **27**, 9166–9174.

Hehre, W.J., Radom, L., Schleyer, P.v.R. & Pople, J.A. 1986 *Ab Initio molecular orbital theory*. New York: John Wiley & Sons.

Hui, S.W. & He, N.B. 1983 Molecular organisation in cholesterol-lecithin bilayers by X-ray and electron diffraction measurements. *Biochemistry* **22**, 1159–1164.

Impey, R.W., Madden, P.A. & McDonald, I.R. 1982 Spectroscopic and transport properties of water. Model calculations and the interpretation of experimental results. *Molec. Phys.* **46**, 513–539.

Janiak, M.J., Small, D.M. & Shipley, G.G. 1979 Temperature and compositional dependence of the structure of hydrated dimyristoyl lecithin. *J. biol. Chem.* **254**, 6068–6078.

Jonas, J., DeFries, T. & Wilbur, D.J. 1976 Molecular motions in compressed liquid water. *J. chem. Phys.* **65**, 582–588.

Jönsson, B., Edholm, O. & Teleman, O. 1986 Molecular dynamics simulations of a sodium octanoate micelle in aqueous solution. *J. chem. Phys.* **85**, 2259–2271.

Jorgensen, W.L. 1989 Free energy calculations: a breakthrough for modelling organic chemistry in solution. *Acc. chem. Res.* **22**, 184–189.

Jorgensen, W.L. 1991 BOSS version 3.1. Yale University, New Haven, Connecticut, U.S.A.

Jorgensen, W.L., Briggs, J.M. & Contreras, M.L. 1990 Relative partition coefficients for organic solutes from fluid simulations. *J. phys. Chem.* **94**, 1683–1686.

Jorgensen, W.L., Chandrasekhar, J., Madura, J., Impey, R.W. & Klein, M.L. 1983 Comparison of simple potential functions for simulating liquid water. *J. chem. Phys.* **79**, 926–935.

Jorgensen, W.L. & Tirado-Rives, J. 1988 The OPLS potential functions for proteins. Energy minimisations for crystals of cyclic peptides and crambin. *J. Am. chem. Soc.* **110**, 1657–1666.

Karaborni, S., van Os, N.M., Esselink, E. & Hilbers, P.A.J. 1993 Molecular dynamics simulations of oil solubilisation in surfactant solutions. *Langmuir* **9**, 1175–1178.

Klose, C. & Gawrisch, K. 1981 Lipid-water interactions in model-membranes. *Studia Biophysica* **84**, 2122.

Levy, R.M., Karplus, M. & McCammon, J.A. 1979 Diffusive Langevin dynamics of model alkanes. *Chem. Phys. Lett.* **65**, 411.

Lewis, B.A. & Engelman, D.M. 1983 Lipid bilayer thickness varies linearly with acyl chain length in fluid phosphatidylcholine vesicles. *J. molec. Biol.* **166**, 211–217.

Lis, L.J., McAlister, M., Fuller, N., Rand, R.P. & Parsegian, V.A. 1982 Interactions between neutral phospholipid bilayer membranes. *Biophys. J.* **37**, 657–666.

Madden, P.A. & Impey, R.W. 1986 Dynamics of coordinated water: a comparison of experiment and simulation results. *Ann. N.Y. Acad. Sci.* **482**, 91114.

Mayer, C., Müller, K., Weisz, K. & Kothe, G. 1988 Deuteron N.M.R. relaxation studies of phospholipid membranes. *Liq. Cryst.* **3**, 797–806.

Meier, P., Ohmes, E. & Kothe, G. 1986 Multipulse dynamic nuclear magnetic resonance of phospholipid membranes. *J. chem. Phys.* **85**, 3598–3614.

Meier, P., Ohmes, E., Kothe, G., Blume, A., Weldner, J. & Elbl, H.J. 1983 Molecular order and dynamics of phospholipid membranes. A deuteron magnetic resonance study employing a comprehensive line-shape model. *J. phys. Chem.* **87**, 4904–4912.

Mendelsohn, R., Davies, M.A., Brauner, J.W., Schuster, H.F. & Dluhy, R.A. 1989 Quantitative determination of conformational disorder in the acyl chains of phospholipid bilayers by infrared spectroscopy. *Biochemistry* **28**, 8934–8939.

Mendelsohn, R., Davies, M.A., Schuster, H.F., Xu, Z. & Bittman, R. 1991 CD_2 rocking modes as quantitative probes of one-, two-, and three-bond conformational disorder in dipalmitoylphosphatidylcholine and dipalmitoylphosphatidylcholine/cholesterol mixtures. *Biochemistry* **30**, 8558–8563.

Meraldi, J.P. & Schlitter, J. 1981 A statistical mechanical treatment of fatty acyl chain order in phospholipid bilayers and correlation with experimental data. *Biochim. biophys. Acta* **645**, 193–210.

Moller, M.A., Tildesley, D.J., Kim, K.S. & Quirke, N. 1991 Molecular dynamics simulation of a Langmuir-Blodgett film. *J. chem. Phys.* **94**, 8390–8401.

Nagle, J.F. & Wilkinson, D.A. 1978 Lecithin bilayers. Density measurements and molecular interactions. *Biophys. J.* **23**, 159–175.

Oldfield, E., Meadows, M., Rice, D. & Jacobs, R. 1978 Spectroscopic studies of specifically deuterium labelled membrane systems. Nuclear magnetic resonance investigation of the effects of cholesterol in model systems. *Biochemistry* **17**, 2727–2740.

Pearson, R.H. & Pascher, I. 1979 The molecular structure of lecithin dihydrate. *Nature, Lond.* **281**, 499–501.

Peng, Z.Y., Simplaceanu, V., Lowe, I.J. & Ho, C. 1988 Rotating-frame relaxation studies of slow motions in fluorinated phospholipid model membranes. *Biophys. J.* **54**, 8195.

Pink, D.A., Green, T.J. & Chapman, D. 1980 Raman scattering in bilayers of saturated phosphatidylcholines. Experiment and theory. *Biochemistry* **19**, 349–356.

Pomès, R. & McCammon, J.A. 1990 Mass and step length optimisation for the calculation of equilibrium properties by molecular dynamics simulation. *Chem. Phys. Lett.* **166**, 425–428.

Raghavan, K., Reddy, M.R. & Berkowitz, M.L. 1992 A molecular dynamics study of the structure and dynamics of water between dilauroylphosphatidylethanolamine bilayers. *Langmuir* **8**, 233–240.

Reynolds, C.A., Essex, J.W. & Richards, W.G. 1992 Atomic charges for variable molecular conformations. *J. Am. chem. Soc.* **114**, 9075–9079.

Rigaud, J.L., Gary-Bobo, C.M. & Lange, Y. 1972 Diffusion processes in lipid-water lamellar phases. *Biochim. biophys. Acta* **266**, 7284.

Rommel, E., Noack, F., Meier, P. & Kothe, G. 1988 Proton spin relaxation dispersion studies of phospholipid membranes. *J. phys. Chem.* **92**, 2981–2987.

Ryckaert, J.P., Ciccotti, G. & Berendsen, H.J.C. 1977 Numerical integration of the Cartesian equations of motion of a system with constraints: molecular dynamics of n-alkanes. *J. comput. Phys.* **23**, 327–341.

Scott, H.L. 1984 Phosphatidylcholine head groups can induce short-range order in interfacial water in vesicles. *Chem. phys. Lett.* **109**, 570–573.

Seelig, J., Gally, H.U. & Wohlgemuth, R. 1977 Orientation and flexibility of the choline head groups in phosphatidylcholine bilayers. *Biochim. biophys. Acta* **467**, 109–119.

Seelig, A. & Seelig, J. 1974 The dynamic structure of fatty acyl chains in a phospholipid bilayer measured by deuterium magnetic resonance. *Biochemistry* **13**, 4839–4845.

Shelley, J.C., Sprik, M. & Klein, M.L. 1993 Molecular dynamics simulation of an aqueous sodium octanoate micelle using polarisable surfactant molecules. *Langmuir* **9**, 916–926.

Shepherd, J.C.W. & Büldt, G. 1978 Zwitterionic dipoles as a dielectric probe for investigating head group mobility in phospholipid membranes. *Biochim. biophys. Acta* **514**, 8394.

Singh, U.C., Weiner, P.K., Caldwell, J.W. & Kollman, P.A. 1988 AMBER version 3.1. Department of Pharmaceutical Chemistry, University of California, San Francisco, California, U.S.A.

Skarjune, R. & Oldfield, E. 1979 Physical studies of cell surface and cell membrane structure. Determination of phospholipid head group organisation by deuterium and phosphorus nuclear magnetic resonance spectroscopy. *Biochemistry* **26**, 5903–5909.

Small, D.M. 1986 *The physical chemistry of lipids: from alkanes to phospholipids*. New York: Plenum Press.

Stouch, T.R., Ward, K.B., Altieri, A. & Hagler, A.T. 1991 Simulations of lipid crystals: characterisation of potential energy functions and parameters for lecithin molecules. *J. comput. Chem.* **12**, 1033–1046.

Stouch, T.R. & Williams, D.E. 1992 Conformational dependence of electrostatic potential derived charges of a lipid headgroup: glycerylphosphorylcholine. *J. comput. Chem.* **13**, 622–632.

Strenk, L.M., Westerman, P.W. & Doane, J.W. 1985 A model of orientational ordering in phosphatidylcholine bilayers based on conformational analysis of the glycerol backbone region. *Biophys. J.* **48**, 765–773.

Stryer, L. 1988 *Biochemistry*, 3rd edn. New York: W.H. Freeman and Company.

Thurmond, R.L., Dodd, S.W. & Brown, M.F. 1991 Molecular areas of phospholipids as determined by ^2H NMR spectroscopy. Comparison of phosphatidylethanolamines and phosphatidylcholines. *Biophys. J.* **59**, 108–113.

Van der Ploeg, P. & Berendsen, H.J.C. 1982 Molecular dynamics simulation of a bilayer membrane. *J. chem. Phys.* **76**, 3271–3276.

Van der Ploeg, P. & Berendsen, H.J.C. 1983 Molecular dynamics of a bilayer membrane. *Molec. Phys.* **49**, 233–248.

Van Gunsteren, W.F. & Karplus, M. 1982 Effect of constraints on the dynamics of macromolecules. *Macromolecules* **15**, 1528–1544.

Weiner, S.J., Kollman, P.A., Case, D.A., Singh, U.C., Ghio, C., Alagona, G., Profeta, S. & Weiner, P. 1984 A new force field for molecular mechanical simulation of nucleic acids and proteins. *J. Am. chem. Soc.* **106**, 765–784.

PHILOSOPHICAL TRANSACTIONS OF THE ROYAL SOCIETY B BIOLOGICAL SCIENCES

Wendoloski, J.J., Kimatian, S.J., Schutt, C.E. & Salemme, F.R. 1989 Molecular dynamics simulation of a phospholipid micelle. *Science, Wash.* **243**, 636–637.

Zaccai, G., Büldt, G., Seelig, A. & Seelig, J. 1979 Neutron diffraction studies on phosphatidylcholine model membranes. II. Chain conformation and segmental disorder. *J. molec. Biol.* **134**, 693–706.

Received 16 August 1993; accepted 21 December 1993

APPENDIX 1. NON-STANDARD AMBER INTRAMOLECULAR PARAMETERS

Table A1. *Angle-bending intramolecular parameters*

(The parameters are used in the potential energy equation: $V = K_\theta\ (\theta - \theta_{eq})^2$.)

angle	K_θ/(kcal mol^{-1} rad^{-2})	θ_{eq}/deg
C—OS—CH	83.0	116.9
C—OS—C2O	83.0	116.9
O—C—OS	83.0	123.4
OS—C—C2	81.0	111.4

Table A2. *Bond-stretching intramolecular parameters*

(The parameters are used in the potential energy equation: $V = K_r\ (r - r_{eq})^2$.)

bond	K_r/(kcal mol^{-1} Å^{-2})	r_{eq}/Å
C—OS	214.0	1.327

Table A3. *Improper dihedral intramolecular parameters*

(The parameters are used in the potential energy equation: $V = \Sigma(V_n/2)\ (1 + \cos(n\phi - \gamma))$, where the summation is performed over n. Idiv is the factor by which the dihedral energy is divided.)

improper dihedral	idiv	$(V_n/2)$/(kcal mol^{-1})	γ/deg	n
OS—C—O—C2	2	42.0	180.0	2.0
OS—C2)—CH—C2O	1	14.0	180.0	3.0

Table A4. *Dihedral intramolecular parameters*

(The parameters are used in the potential energy equation: $V = \Sigma(V_n/2)\ (1 + \cos(n\phi - \gamma))$, where the summation is performed over n. Idiv is the factor by which the dihedral energy is divided.)

dihedral	idiv	$(V_n/2)$/(kcal mol^{-1})	γ/deg	n
C2O—OS—C—C2	1	−0.086	0.0	1
C2O—OS—C—O	1	4.084	180.0	2
CH—OS—C—C2	1	−0.086	0.0	1
CH—OS—C—O	1	4.084	180.0	2

PHILOSOPHICAL TRANSACTIONS OF THE ROYAL SOCIETY B BIOLOGICAL SCIENCES